THE UNIVERSITY OF CHICAGO

FROM MOLECULAR ELECTRONICS TO QUANTUM CONTROL - REDUCED DENSITY MATRIX APPROACH

A DISSERTATION SUBMITTED TO
THE FACULTY OF THE DIVISION OF THE PHYSICAL SCIENCES
IN CANDIDACY FOR THE DEGREE OF
DOCTOR OF PHILOSOPHY

DEPARTMENT OF CHEMISTRY

BY
MANAS SAJJAN

CHICAGO, ILLINOIS
DECEMBER 2018

To Maa and Baba

TABLE OF CONTENTS

LIST OF FIGURES

LIST OF TABLES

ABSTRACT

Over the past few decades, constrained minimization of the energy with respect to the two-electron reduced-density-matrix (2-RDM) has emerged as a tantalizing alternative to study electronic structure of strongly correlated molecular and atomic systems at favorable polynomial scaling. In this thesis, we extend this variational minimization procedure to conducting systems in presence of a non-zero charge flux to mimic situations in single-molecular devices. We replicate the exponential length scaling of zero-bias conductance in off-resonant tunnelling dominated transport in oligoacenes (with a reasonable estimate of the decay constant) and even the trend reversal due to orientation flipping, all from the intrinsic features of the systems. When the method is applied to benchmark cases like 1,4-benzenedithiol clipped with Au electrodes, we see that unlike current theoretical standards, the theory does not over-predict the conductance by orders of magnitude compared to experimental results. In fact it is even consistent with all trends seen with respect to changing electrodes, linkers and chemical substitution over the molecular backbone studied experimentally over the years. The technique was also applied to a binuclear vanadium complex and its positively charged state known to exhibit Kondo resonance. We see that both the partners offers multiple orbital degeneracies necessitating important multi-reference effects completely missed in the previous interpretation of the experiment based on model Hamiltonians. Such strongly correlated cases are untreatable by transport methodologies based on DFT. We not only reproduce the conductance trend seen experimentally but highlight the importance of many-body analysis in enhancing the Kondo features. We also apply the method to study switching action in pH sensors identifying the role of energetics and zero-field polarizability in controlling the conductance of the 'on' and 'off' states of the switch. Lastly we study the effect of spatially homogeneous electric field in altering quantum correlations and entanglement in molecular systems and interpret the results using geometric arguments.

ACKNOWLEDGMENTS

Trepidations associated with a daunting task like PhD would have been overwhelming without the love and support of a number of important people in my life who I would take this opportunity to acknowledge.

Firstly, I express my sincere gratitude to the most important man behind this i.e. my supervisor Prof. David A. Mazziotti for having faith in me and being a constant source of guidance through every phase of this journey. His tireless support throughout the last five years has been the primary source of inspiration that ensured the completion of this work. Extension of reduced density matrix method from the familiar domain of electronic structure to a new direction like transport has often been a rugged road. But even when success seemed a far-fetched dream his enthusiasm and outlook towards science was infectious and served as a fuel that kept me motivated. His mentor-ship style enhanced my growth on every aspect of scientific research which not only included learning the tricks of the trade but also lucid presentation and simplified yet effective communication of results. I would thereby thank you from the bottom of my heart for all those hours of discussions and your perspicacious inputs which always reaffirmed the direction. I would also thank Prof. Timothy C. Berkelbach and Prof. Gregory S. Engel for evaluation of this work and for consenting to be on my dissertation committee. Discussion with Prof. Berkelbach on the topics concerning this thesis has been helpful in presenting the key ideas.

I would also like to thank Prof. Tian Bozhi, Prof. Andrei Tokmakoff, Prof. Greg Engel, Prof. David Mazziotti and Prof. Greg Voth for all the wonderful courses they taught during my first year in UChicago which has served as a great stepping stone to research. Occasional discussions with Prof. Tian Bozhi on the hallway of JFI even late at night has been fun, inspiring and motivational always. Prof. David Schuster had been a friendly face when we shared neighboring offices. The innumerable discussions with Prof. Harvey and Late Prof. Kadanoff on topics extending all length and energy scales like birth and death of neutron stars and quantum gravity to spin Hall effect has been fascinating and a great learning

experience. Kudos must also go out to my students who not only made my first year in UChicago fun but continues to be great friends even now. A big thank you to my all my friends and classmates (Michael, Luke, Joseph, Dan, Erik,Anthony, Darren, Nick, Preston, Jeff, Sarah, Morris) for the exciting times when we shared the Kent offices.

I would also express my sincere regards to all past and present members of the Mazziotti group (Srikant, Chad, Andrew Sand, Erik Hoy, Nick, Romit, Valentine, Erica, Alison, Ali, Kade, Lexie, Claire, Shining, Anthony, Shayan, Shiva, Jason, Jackie, Olivia, Jan Niklas, Scott, Simon and Ezraa) for making the experience fun-filled and exciting. Alison in particular continues to be a wonderful friend and source of support who I shall treasure for the rest of my life. Together we have had lots of discussions and spent many wonderful evenings. I will definitely miss the innumerable scientific discussions with Valentine from which I benefited immensely and the friendly banter with Anthony, Kade and Ali and later on with Shiva. In the later years Shayan has been a great friend and together we not only had many mutually beneficial scientific and personal discussions (not to mention the movie nights) but a number of fruitful collaborative ventures. Outside the lab, Johnny has been my closest friend and confidante who I shall continue to look up to. He always made sure to stand by me in good and bad times. Memories of the dinners we spent together especially those with his family are some of my favorites in Chicago. Similarly, Erik has been another very close buddy with whom I had lot of enriching discussions. I will never forget the wonderful evening I spent with his family or the fun we had at his wedding. Karen, Brenda and Maria have always been friendly faces who extended all help and administrative support whenever we needed any.

A big thank you to the Indian contingent in UChicago (Piyush, Kushal, Sayar, Soudeep, Vishwas, Preeti, Subhadip, Debshouri, Krithika, Bodhi, Upasana, Vishnu, Aneesh, Maulik, Bhavya, Shareefa, Krishna, Ankur, Sohail, Aniket, Rishideep, Sabyasachi, Anand, Kasturi, Shiva, Saurja, Ananth and Nagarjuna) for adding humor to the last five years. Together we had many fun-filled moments that I shall always treasure. A special thank you to Subhajit

da and Sayoni di (not to mention the numerous scientific and intellectual discussions we three had) both of whom continues to be my friend, confidante and mentor and my source of support through thick and thin. A special mention should also be extended to Rahul Bhaiyya and Anwesha di who always showered their brotherly affection on me and together with Sayoni di is inarguably an extension of my family now. My journey in Chicago is unimaginable without any of them.

A big shout out to my friends in India (Navendu, Arka, Deep, Rahul, Prasenjit, Nairhita, Sougoto, Kaustav, Tamal, Utsab, Sankar, Agasti) whose undying support and unconditional love and concern towards my well being even during my rough phases has kept me going. They are too precious to me even say a thank you as I know they will always be there. My friends elsewhere in the United States (Supriya and Sanjay) have always extended their helping hand, advices and encouragement both during good and challenging times. Supriya in particular has been more than a brother and continues to be my rock for steady support. I always look up to him for suggestions both professional and personal. Lot of good things in my life have been initiated by him for which I shall remain forever indebted.

I would also take this opportunity to express my gratitude and regards to all my previous teachers and mentors without whom I would not have made this far. The seeds for my early interest in Physical Chemistry was skillfully sown by my high school teacher and very first motivator Mrs. Sharmila Goswami, who continue to be a source of support even after so many years. This was further nurtured and groomed by the excellent team of professors in St.Xaviers. In particular Prof.Indranil Chakraborty has always been a fatherly figure, a friend, a mentor, a guide who I can share anything with. He never turned away from giving me his sagacious advices on all aspects of my life and career and continues to be concerned about my well-being always. I extend my regards to Prof. Anindya Datta (IITB) for inspiring me and teaching me the rudiments of scientific research and always having faith and high aspirations on me. He has been a mentor in true sense who I shall always continue to turn to solicit advices. I extend my recognition to Prof.Rajarshi Chakraborty

(IITB) with whom I have had many exciting and fruitful scientific and personal discussions and who continues to inquire about my well-being from time to time. A special mention to Prof.D.S. Ray (IACS) for mentoring me during my summer internships with his profound knowledge and wisdom and nurturing my interest towards theoretical research. A big thank you to all of you. This degree is as much yours as is mine.

I would like to thank my family especially Maa and Baba whose unconditional sacrifices in raising me which often involved stretching beyond their means. Their undying support and love has equipped me to be capable of withstanding all tumultuous times. I love you all above everything (and my little nephew Rishan who has been a source of joy for the last few years) and dedicate this thesis entirely to you two.

Lastly I would also like to dedicate this thesis to all those students who find elegance in mathematical representations of physical laws.

CHAPTER 1

INTRODUCTION

For a pure-state in a quantum-mechanical system every statistical description like the probabilistic outcomes of a measurement of any property, the post measurement state and the average (expectation) value of the property associated with several observations are all encoded in the wave-vector of the system customarily denoted by $|\Psi\rangle$. In absence of relativistic corrections, the equation of motion of the said vector resolved in the position basis (called the wave-function $\Psi(\vec{r},t)$) is governed by the Schrödinger equation

$$i\hbar\frac{\partial}{\partial t}\Psi(\vec{r},t) = \hat{H}(\vec{r},t)\Psi(\vec{r},t) \tag{1.1}$$

where t is the time, and $\hat{H}$ is the Hamiltonian. The Hamiltonian, which acts as the generator of time-translation as above, in position space representation (in absence of relativistic terms and spin-orbit coupling) is given by

$$\hat{H}(\vec{r},t) = \sum_{i}^{N} -\frac{\hbar^2}{2m_i}\nabla_i^2 + V(\vec{r},t). \tag{1.2}$$

The first term in Eq.1.2 is the sum of the kinetic energy of each particle in the system, and $V(\vec{r},t)$ is potential energy term. The usual solution to Eq.1.1 for a *time-independent Hamiltonian* ($V(\vec{r},t) = V(\vec{r})$) as we concern ourself in this thesis is

$$\Psi(\vec{r},t) = \exp(-\hat{H}(\vec{r})t/\hbar)\Psi(\vec{r},0) \tag{1.3}$$

where $\Psi(\vec{r},0)$ is the initial state of the system which can be resolved in any complete basis. If the $\hat{H}(\vec{r})$ is Hermitian, the above time translation being unitary conserves particle number in the system. Also diagonalizing such a Hermitian Hamiltonian yields a complete basis $\{\Phi_j(\vec{r})\}$ as follows:

$$\hat{H}(\vec{r})\Phi_j(\vec{r}) = E_j\Phi_j(\vec{r}) \tag{1.4}$$

where the eigenvalue (E_j) is the corresponding energy to each $\Phi_j(\vec{r})$. An arbitrary initial state $\Psi(\vec{r}, 0)$ can now be resolved in this basis as :

$$\Psi(\vec{r}, 0) = \sum_j C_j\Phi_j(\vec{r}) \tag{1.5}$$

with C_j being the coefficients of the resolution. Substituting Eq.1.5 in 1.3 followed by time translation would allow a complete description of the system at all times. Thus much of non-relativistic quantum mechanics concerns itself with diagonalizing the Hamiltonian $\hat{H}(\vec{r})$ to obtain the set $\{\Phi_j(\vec{r})\}$ which are called the stationary states of the system due to their phase-like time evolution.

In particular, electronic structure seeks the solution for a special class of $\hat{H}(\vec{r})$ consisting of interactions between positively charged nuclei and negatively charged electrons and the mutual repulsion between the like charges. For these systems (with no relativistic corrections or spin-orbit coupling) under Born-Oppenheimer approximation where the massive nuclei are considered effectively stationary thereby decoupling the electronic and nuclear motion, the electronic part of the Hamiltonian reads:

$$\hat{H} = \sum_i^N -\frac{\hbar^2}{2m_i}\nabla_i^2 + \sum_i^N\sum_I^M \frac{-1}{|\vec{r_i} - \vec{R_I}|} + \sum_{i<j}^N \frac{1}{|\vec{r_i} - \vec{r_j}|}. \tag{1.6}$$

The first term contains the kinetic energy of the electrons, the second term contains the attractive interaction between the frozen nuclei (with co-ordinates designated as $\vec{R_I}$) and the electrons and the third term is the electron-electron repulsion (with co-ordinates designated as $\vec{r_i}$). Obtaining the many-body stationary states (hence any arbitrary state from Eq.1.5 and 1.3) of the above Hamiltonian and its corresponding energies together with the restriction that the said states will be anti-symmetric under permutation of indices (respecting the fact

electrons are indistinguishable fermions with s=1/2), defines the goal of almost all electronic structure methods.

1.1 Mean field treatment-Hartree Fock method

Due to the two-body electron-electron repulsion term, an exact solution to the eigenstates of the electronic Hamiltonian is not possible for more than one electron, and therefore approximate numerical methods are constructed. Using variational theorem one can thus approximate the stationary states with a valid guess. To ensure the anti-symmetry property the simplest guess would be to use a single N-electron Slater determinant as the trial wavefunction. The corresponding method is called Hartree-Fock theory [1] which physically involves assuming each electron to move in a combined average field of all other electrons and the nucleus. A single-Slater determinant is

$$|\Phi\rangle = \frac{1}{\sqrt{N!}} \begin{vmatrix} \phi_1(1) & \phi_2(1) & \cdots & \phi_N(1) \\ \phi_1(2) & \phi_2(2) & \cdots & \phi_N(2) \\ \vdots & & \ddots & \vdots \\ \phi_1(N) & \phi_2(N) & \cdots & \phi_N(N) \end{vmatrix} \tag{1.7}$$

where ϕ_i is the ith orthonormal one-particle function (often called orbitals). Substituting the above ansatz into the energy expression from the many-body Hamiltonian in Eq.1.6 followed by a variational minimization of the energy with respect to the orbitals subject to orthonormality necessitates that the orbitals are eigenvectors of the following Fock operator

$(\phi_i(x_1))$:

$$
\begin{aligned}
f_i\phi_i(x_1) &= (h_i(x_1) + \sum_j J_j(x_1) - \sum_j K_j(x_1))\phi_i(x_1) = \epsilon_i\phi_i(x_1) \qquad (1.8)\\
J_j(x_1) &= \int_{x_2} \phi_j^*(x_2)|1/|r_{12}|\phi_j(x_2)dx_2 \\
K_j(x_1)\phi_i(x_1) &= \int_{x_2} \phi_j^*(x_2)|1/|r_{12}|\sigma_{12}\phi_j(x_2)\phi_i(x_1)dx_2
\end{aligned}
$$

where σ_{12} is a transposition operator permuting two indices. Since the Fock operator itself depends on its eigenvectors, the method involves starting with an initial guess for each $\phi_i(x_1)$ resolving it in the basis of AOs (approximated by gaussians usually) and then solved iteratively until self-consistency in density is achieved. The N electrons are placed in the lowest energy N molecular orbitals $(\phi_i(x_1))$ produced from the converged procedure to obtain the ground state determinant. Due to its simplicity, the scaling of HF method is $\mathcal{O}(r^3)$ where r is the single-particle basis rank. Also for simple sigma-bonded systems at equilibrium geometry, HF frequently captures more than 90% of the total electronic energy which makes it a starting point for most advanced electronic structure methods.

1.2 Electronic Correlation and Post-Hartree Fock Methods

The HF state mentioned above is the eigenstate of the many-body Fock operator $F = \sum_i f_i$ and not of the actual Hamiltonian in Eq.1.6. In general HF assumes the electrons to be interacting with a mean-field cloud of all other electrons whereas in reality the interaction is instantaneous which can result in a significant change in the trajectories of electrons in a quest to avoid each other. This gives rise to coordinated motion which is not accountable in a single-determinantal state. Mathematically, since the fock-operator in Eq.1.8 is hermitian, its eigenvectors (the orbitals) are guaranteed orthonormal (the degenerate ones can be orthogonalized). The determinants formed from these orbitals are therefore endowed with the

same property and hence can act as a many-body basis for the multi-electron state. Thus a linear combination of all possible determinants of all N electrons placed into all r orbitals would yield the exact ground state of the Hamiltonian in Eq.1.6 in the chosen one-particle basis. This is known as the full configuration interaction (full CI) [2].

$$|\Phi_{FCI}\rangle = c_0|\Phi_0\rangle + \sum_{ia} c_i^a|\Phi_i^a\rangle + \sum_{\substack{i<j \\ a<b}} c_{ij}^{ab}|\Phi_{ij}^{ab}\rangle + \dots \tag{1.9}$$

where $|\Phi_0\rangle$ is the HF-ground state defined in previous section and $|\Phi_{\{p\}}^{\{q\}}\rangle$ is the determinant produced by moving electrons out of the occupied $\{p\}$ orbitals in the HF ansatz into the unoccupied $\{q\}$ orbitals. The energy of this wavefunction is denoted by E_{FCI}. Diagonalizing the many-body Hamiltonian in Eq.1.6 in the basis of these determinants using Eq.1.9 as the ansatz not only yields the ground many body state but also the excited states with suitable choices of the coefficients $\{c\}$. Since such an ansatz allows interaction between various configurations (determinants) it can recover full-correlation in the system. The difference in energy $E_{FCI} - E_{HF}$ is consequently called the correlation energy(E_{corr}). The value of the correlation energy is usually very high for systems with quasi-degenerate π manifold, distorted geometries and in events of bond-breaking and reformation where much of chemistry happens which highlights its significance. Unfortunately, full CI scales combinatorially as rC_N (the determinants are further spin-adapted to respect spin symmetry), which limits its usablility to systems with 16-18 electrons and 16-18 spatial orbitals only. Beyond this the method is intractable.

Thus much of electronic structure is devoted to developing smarter and inexpensive algorithms that capture as much of the correlation energy as possible and yield the closest approximation to the ground and excited states to the FCI state. A straight-forward yet tractable extension will be to truncate the wavefunction in Eq.1.7 up until a certain excitation order [3]. Unfortunately, truncated CI methods are not size-extensive(the energy of a supermolecule consisting of N non-interacting copies of the initial molecule is not equal to

N times the energy of each) or size-consistent (the molecule under dissociation limit do not possess the energy of the collective sum of the right dissociated fragments). Size-extensive approximations to full CI such as Møller-Plesset perturbation theory [4] are also possible which being dependant on the single-reference Hartree Fock state recovers a great deal of dynamic correlation. However the method being non-variational is not guaranteed to converge with higher order corrections included. Instead of a linear excitation operator as is used in truncated CI, if one uses an exponential excitation tensor like in coupled-cluster theory [5], the accuracy can be greatly improved even with lesser number of excitations (and hence low cost). The method also retains size-consistency as higher order excitations are often approximated in terms of lower order ones. The method with single and double excitations with perturbative triples, CCSD(T), is ubiqutously used and often considered to be of benchmark accuracy [6] with a scaling of $\mathcal{O}(r^7)$. Even though multi-reference extensions of this technique exists, but the far more common variety depends on a single-HF reference and may struggle for convergence and accuracy when multiple quasi-degenerate determinantal configurations are possible making it ambiguous to even define a reference (non-dynamic correlation) For such systems, an active space CI which entails inclusion of all determinants generated by excitations within a certain subset of orbitals and also unitarily transforming the orbitals themselves so that they imbibe each others character also exists and is called CASSCF [7]. Such a wavefunction can then act as a reference for further recovery of dynamical correlation as in perturbation theory methods and coupled cluster [8]. However due to operational similarity, the scaling of CASSCF is exponential like the FCI which restricts it to be usable only for a small active space size.

A completely different class of method which optimizes the ground state energy with respect to one-particle density also exists and is called Density Functional Theory(DFT) (see chapter 2). This has been ubiqutously used not only for atoms and molecules but for condensed phases like solids and liquids too due to its similar scaling to HF $\mathcal{O}(r^3)$. However due to its single-reference operational framework, the method struggles with cases with

multiple equally plausible configurations.

Even though conceptually similar but operationally a completely different method based on reduced density matrices have also been developed over the years with polynomial scaling which being independent of reference is particularly suited for recovering non-dynamic correlation. These will be elaborated in the following section.

1.3 Reduced-Density-Matrix Methods

Let us introduce a set of operators $a_p^\dagger$ and a_p which creates and annihilates an electron in the orbital p, respectively such that they satisfy the following algebra:

$$\{a_p^\dagger, a_q^\dagger\} = 0 \tag{1.10}$$

$$\{a_q, a_p^\dagger\} = \delta_p^q \tag{1.11}$$

Using the definition of these operators as $a_p^\dagger|0\rangle = |p\rangle$ and $a_p|p\rangle = |0\rangle$ it is possible to write the electronic Hamiltonian in Eq.1.7 as

$$\hat{H} = \sum_{\substack{i<j \\ l<k}} {}^2K_{kl}^{ij} a_i^\dagger a_j^\dagger a_l a_k \tag{1.12}$$

where ${}^2K_{kl}^{ij}$ contains the one- and two-electron integrals

$$\begin{aligned}
{}^2K_{kl}^{ij} &= \frac{1}{N-1}(\delta_{ik}\langle j|\hat{h}|l\rangle + \delta_{lj}\langle i|\hat{h}|k\rangle) + \langle ij|\hat{V}|kl\rangle. \\
\langle i|\hat{h}|k\rangle &= \langle i|\frac{\hbar^2}{2m}\nabla^2 + \sum_I^M \frac{-1}{|\vec{r_1} - \vec{R_I}|}|k\rangle \\
\langle ij|\hat{V}|kl\rangle &= \frac{1}{2}\langle ij|\frac{1}{|\vec{r_1} - \vec{r_2}|}|kl\rangle
\end{aligned}$$

The energy of a pure stationary state of the Hamiltonian (representable by a wavefunction) $|\Phi\rangle$ is given by

$$\begin{aligned} E &= \langle\Phi|\hat{H}|\Phi\rangle \\ &= \sum_{\substack{i<j \\ l<k}} {}^2K_{kl}^{ij}\langle\Phi|a_i^\dagger a_j^\dagger a_l a_k|\Phi\rangle. \\ &= \mathrm{Tr}({}^2K^2D) \end{aligned} \tag{1.13}$$

where

$${}^2D_{kl}^{ij} = \langle\Phi|a_i^\dagger a_j^\dagger a_l a_k|\Phi\rangle \tag{1.14}$$

The above equation states that the energy can be exactly expressed as a function of the 2-RDM, because the Hamiltonian only contains one- and two-particle operators and the electrons are indistinguishable. In general for any p-particle operator, the pth-order RDM obtained by integrating all (N-p) space-spin variables from the N-body density matrix is required. For the energy functional, the knowledge of the 2-RDM suffices and since it contains lot less information than the exact many-body ground state of the Hamiltonian (Φ_{FCI}), the direct minimization of the energy with respect to the elements of the 2-RDM [9]. is extendable to larger systems of chemical interest and should in principle recover a great deal of correlation energy.

1.3.1 N-representability

It was established early that such an unconstrained direct minimization yields energies that are far too low [10, 11]. This is because while every N-particle density matrix may be contracted to a 2-RDM but in absence of knowledge of the N-particle state, the 2-RDM matrix elements obtained directly from the unrestricted optimization scheme may not represent a realistic N-particle density matrix as a pre-image. This is known as the N-representability problem [9].The set of all possible 2-RDMs is therefore being much larger than those derivable from an N-electron density matrix (or wavefunction for pure states) and hence energy

minimizations with respect to the 2-RDM acts as a lower bound to the full CI energy.

The eigenvalues of the 2-RDM, gives the probability of finding two electrons in a given antisymmetric two-electron geminal. Since such probabilities cannot be negative, an important N-representability conditions of the 2-RDM enforced during optimization is its positive semidefiniteness.

$$^2D \succeq 0 \tag{1.15}$$

These constraints should also be shared by the two other metric matrices in two-particle space namely the two-hole (^2Q) and one-particle-one-hole matrices (^2G).

$$\begin{aligned} {}^2Q^{ij}_{kl} &= \langle\Phi|\hat{a}_i\hat{a}_j\hat{a}^\dagger_l\hat{a}^\dagger_k|\Phi\rangle \succeq 0 \\ {}^2G^{ij}_{kl} &= \langle\Phi|\hat{a}^\dagger_i\hat{a}_j\hat{a}^\dagger_l\hat{a}_k|\Phi\rangle \succeq 0 \end{aligned} \tag{1.16}$$

Together they ensure that the probabilities of finding two holes and an electron and a hole in the antisymmetric hole geminal and the excitonic two-body functions to be non-negative. This gives the DQG conditions [12–14] which ensures the above matrices are 2-positive even though not completely N-representable. The energy obtained by enforcing such constraints act as a lower bound to the full-CI energy. Further introduction of constraints are necessary to approach the exact limit. Extension to ensure semi-definiteness of the sum of three particle metric matrices (T2-condition) are also used. The optimization with DQG conditions has a polynomial scaling of $\mathcal{O}(r^6)$ and that with the extra T2 conditions are $\mathcal{O}(r^9)$ which restricts the latter to smaller systems only. Also a 2-positive ^2Q and ^2D ensures that the 1-RDM and the 1-hole RDM obtained from tensor contraction is positive semi-definite too.

$$\begin{aligned} {}^1D^i_k &= \langle\Phi|\hat{a}^\dagger_i\hat{a}_k|\Phi\rangle = \sum_l {}^2D^{il}_{kl} \succeq 0 \\ {}^1Q^i_k &= \langle\Phi|\hat{a}_i\hat{a}^\dagger_k|\Phi\rangle = \sum_l {}^2Q^{il}_{kl} \succeq 0 \\ {}^1D^i_k + {}^1Q^i_k &= \delta^i_k \end{aligned} \tag{1.17}$$

with the last expression being a restatement of Eq.1.11.

1.3.2 Optimization scheme

Thus the final optimization scheme with the DQG conditions becomes

$$\min_{^2D} E[^2D](\quad = \quad \mathrm{Tr}[^2K\ ^2D]) \tag{1.18}$$

$$\text{such that } ^2D \quad \succeq \quad 0 \tag{1.19}$$

$$^2Q \quad \succeq \quad 0 \tag{1.20}$$

$$^2G \quad \succeq \quad 0 \tag{1.21}$$

$$\mathrm{Tr}(A_j\ ^2D) + \mathrm{Tr}(B_j\ ^2Q) \quad + \quad \mathrm{Tr}(C_j\ ^2G) = b_j.\ \forall j \tag{1.22}$$

where the last set of constraints enforce the linear mappings between the two-particle metric matrices . With these constraints the optimization scheme has been known to yield energies that are of high chemical accuracies even for strongly correlated systems[15–18]. An active space formulation of the variational 2-RDM method[19] is extended in Chapter 2,3 to study conducting molecular systems with an internal current flux[20]. In Chapter 4 , along with wavefunction techniques a similar 2-RDM method which involves parameterizing the 2-RDM elements in terms of a CISD wavefunction [21] with size-extensivity and partial-N-representability [22, 23] is used to study the effect of electric field on quantum correlation[24].

1.4 References

[1] A. Szabo and N. S. Ostlund, *Modern Quantum Chemistry: Introduction to Advanced Electronic Structure Theory* (Dover, New York, 1996).

[2] I. Shavitt, *The Method of Configuration Interaction* (Springer US, Boston, MA, 1977), pp. 189–275.

[3] C. D. Sherrill and H. F. Schaefer III (Academic Press, 1999), vol. 34 of *Advances in Quantum Chemistry*, pp. 143 – 269.

[4] C. Møller and M. S. Plesset, Phys. Rev. **46**, 618 (1934).

[5] I. Shavitt and R. J. Bartlett, *Many-body methods in chemistry and physics: MBPT and coupled-cluster theory* (Cambridge university press, 2009).

[6] J. Rezac and P. Hobza, J. Chem. Theory Comput. **9**, 2151 (2013).

[7] B. O. Roos, P. R. Taylor, P. E. Si, et al., Chem. Phys. **48**, 157 (1980).

[8] P. Piecuch, N. Oliphant, and L. Adamowicz, J. Chem. Phys. **99**, 1875 (1993).

[9] A. J. Coleman, Rev. Mod. Phys. **35**, 668 (1963).

[10] R. H. Tredgold, Phys. Rev. **105**, 1421 (1957).

[11] A. J. Coleman and V. I. Yukalov, *Reduced density matrices: Coulsons challenge*, vol. 72 (Springer Science & Business Media, 2000).

[12] M. Nakata, H. Nakatsuji, M. Ehara, M. Fukuda, K. Nakata, and K. Fujisawa, J. Chem. Phys. **114**, 8282 (2001).

[13] D. A. Mazziotti, Phys. Rev. Lett. **93**, 213001 (2004).

[14] D. A. Mazziotti, Chem. Rev. **112**, 244 (2012).

[15] A. W. Schlimgen, C. W. Heaps, and D. A. Mazziotti, J. Phys. Chem. Lett. **7**, 627 (2016).

[16] J. M. Montgomery and D. A. Mazziotti, The Journal of Physical Chemistry A **122**, 4988 (2018), pMID: 29771514, `https://doi.org/10.1021/acs.jpca.8b00941`, URL `https://doi.org/10.1021/acs.jpca.8b00941`.

[17] L. Greenman and D. A. Mazziotti, J. Chem. Phys. **133**, 164110 (2010).

[18] L. Greenman and D. A. Mazziotti, J. Chem. Phys. **130**, 184101 (2009).

[19] G. Gidofalvi and D. A. Mazziotti, J. Chem. Phys. **129**, 134108 (2008).

[20] M. Sajjan and D. A. Mazziotti, Communications Chemistry **1**, 31 (2018), URL https://doi.org/10.1038/s42004-018-0030-2.

[21] C. Kollmar, J. Chem. Phys. **125**, 084108 (2006).

[22] D. A. Mazziotti, Phys. Rev. Lett. **101**, 253002 (2008).

[23] D. A. Mazziotti, Phys. Rev. A **81**, 062515 (2010).

[24] M. Sajjan, K. Head-Marsden, and D. A. Mazziotti, Phys. Rev. A **97**, 062502 (2018), URL https://link.aps.org/doi/10.1103/PhysRevA.97.062502.

CHAPTER 2

CURRENT-CONSTRAINED VARIATIONAL THEORY- THE FOUNDATIONS

- This chapter contains parts of an article that was originally published in the Communications Chemistry. Reproduced with permission from [M.Sajjan and D. A. Mazziotti, *Communications Chemistry*, **1**, 31 (2018)]. Copyright 2018, Springer Nature.

- This chapter contains parts of several articles that are under preparation at the time of writing.

In this chapter we establish a new theory based on reduced density matrices introduced in the previous chapter. But before we start, lets briefly highlight the present ubiquitously used theoretical standard which involves the marriage of Non-Equlibrium Greens functions (NEGF) in density functional theory framework. In the following section, an overview of density functional theory is presented (DFT) followed by a brief exposition to NEGF. In the last section we present the newly developed theory based on reduced density matrices before moving onto its applications in the next chapter.

2.1 Density Functional Theory (DFT)

Density functional theory (DFT) is one of the most popular and powerful method for computing the ground state properties of many electron systems. Unlike traditional wave-function based methods described in the previous chapter DFT uses the single-particle density $n(r)$ as the fundamental variable which is defined as follows:

$$n(r) = \langle\psi| \sum_{i=1}^{N} \delta(r - r_i)|\psi\rangle. \tag{2.1}$$

This thereby maps the problem for a many-electron system with 3N degrees of freedom into an effective single particle space which reduces the scaling drastically. Each single

electron is assumed to be in a combined mean field of all other associated electrons and the nucleus much like in Hartree-Fock theory. The Hohenberg and Kohn Theorems are responsible for providing the fundamental backbone for this mapping

Hohenberg-Kohn shows [1] that

- For a system of interacting particles in an external potential $V_{ext}(r)$, the single particle density has a unique one to one correspondence with the external potential. This thereby justifies the use of electron density ($n(r)$) to retain all necessary information about the many-body state.

- The energy of the many-particle system can be written in terms of a universal functional of the single particle density and the external potential. This thereby allows to extract the true ground state of the system as the global minimum of this functional. In other words we can write

$$E[n] = F[n] + \int n(r)V_{ext}dr. \tag{2.2}$$

$$E[n] = min(E[n]) \Longleftrightarrow \frac{\delta E[n]}{\delta n}|_{n=n_0} = 0. \tag{2.3}$$

wherein the first term $F[n]$ is a universal functional of the sum of kinetic and coulomb energies and hence depends only on the number of particles in the system and $n_0(r)$ corresponds to the ground state one-electron density obtained from the global minimum energy. These two theorems only provide proof of existence and uniqueness of the functional $F[n]$ without any concrete recipe to evaluate its exact form for any arbitrary system.

W. Kohn and L. Sham (KS) for a practical implementation of DFT mapped the problem of interacting particles in an external potential to an auxillary system of non-interacting

particles with equivalent ground state (non-interacting V representability)[2]. The scheme defines $F[n]$ as follows:

$$F[n] = T[n] + E_H[n] + E_{XC}[n] + E_{ext}[n], \tag{2.4}$$

wherein

$$E_{ext} = \int V_{ext} n(r) dr, \tag{2.5}$$

$$T[n] = -\int \sum_{i=1}^{N} \psi_i^*(r) \frac{\hbar^2 \nabla^2}{2m} \psi_i(r) dr, \tag{2.6}$$

$$E_H = \frac{e^2}{8\pi\epsilon_0} \int \frac{n(r)n(r')}{|r - r'|} dr dr'. \tag{2.7}$$

The exchange-correlation functional $E_{XC}[n]$ is not known exactly for any arbitrary system and will have to be duly approximated. Single-particle density is then obtained from the occupied orbitals ($\psi_{i,\sigma}(r)$) of a single-determinantal Hartree-Fock ansatz as follows:

$$n(r) = \sum_{\sigma}^{i} \psi_{i,\sigma}^*(r) \psi_{i,\sigma}(r). \tag{2.8}$$

Ground-state of the system can be obtained by minimizing energy with respect to $\psi_{i,\sigma}^*(r)$ subject to orthonormality. This necessitates that these orbitals are eigenvectors of the following equation (The Kohn-Sham equation)

$$(-\frac{\hbar^2}{2m}\nabla^2 + V_{eff})\psi_{i,\sigma}(r) = \epsilon_i \psi_{i,\sigma}(r), \tag{2.9}$$

$$V_{eff} = V_{ext} + V_H + V_{XC} = V_{ext} + \int \frac{n(r')}{|r - r'|} + V_{XC}[n(r)], \tag{2.10}$$

where

$$V_{XC} = \frac{\delta E_{XC}[n(r)]}{\delta n(r)}. \tag{2.11}$$

Both V_H and V_{XC} depend on electron density which in turn is obtained from the solution of the problem. One needs to start from an initial guess for the single particle density and then construct the Kohn-Sham Hamiltonian and diagonalize it to obtain the orbitals $\psi_{i,\sigma}(r)$ which in turn is used to construct a new-single density (Eq.2.8) that goes into the next cycle. In this way the problem is solved through number of iterations till self-consistency is achieved which is characterized by a change in single-electron particle density between successive iterations below a certain preset threshold. The energy so obtained after convergence (Eq.2.2) is the many-body ground state energy.

The exchange-correlation (XC) energy functional E_{XC} required to solve the Kohn-Sham equation is in general given by,

$$E_{XC}[n] = \int n(r) f(n(r), \nabla n, ...) dr. \tag{2.12}$$

The simplest form is to approximate it to be a functional of density of a homogenous electron gas (HEG)[3–5]. This is called the Local Density Approximation (LDA). Even though it is good for solids, but for molecules and atoms the results are quantitatively poor and also it suffers from self-interaction error with the Hartree potential term.

The next refinement is making the exchange correlation functional depend not only on

the density of HEG but also on its higher order derivatives. Inclusion of the gradient, $\nabla n(r)$ in the expansion produces the Generalized-Gradient Approximation (GGA) and inclusion of both the gradient and the Laplacian of the density produces the meta-GGA approximation. Hybrid density functionals which are built to include a part of the exact Hartree Fock exchange in the GGA functional are now routinely used and afford a good compromise between accuracy and cost.

2.2 Density Functional Theory and Non-Equilibrium Green's Functions (DFT-NEGF)

While interfacing an electronic structure method to compute transport, one has to carefully take into consideration all the key components of the circuit including the molecular bridge, the semi-infinite contacts (electrodes/reservoirs) and the interaction between the two under finite bias. DFT-NEGF provides a practical scheme to achieve the purpose. The Hamiltonian of the whole molecule-electrode combination (H) is partitioned as follows.

$$H = \begin{bmatrix} H_L & H_{LM} & 0 \\ H_{LM}^{\dagger} & H_M & H_{MR}^{\dagger} \\ 0 & H_{MR} & H_R \end{bmatrix}$$

wherein $H_{L\ R}$ are the Hamiltonian matrix blocks for the left(right)electrodes and H_M is that of the central molecular material which has slices of the electrode too (together called the active region). H_{MR} and H_{LR} denotes the coupling blocks of the active region to the respective electrodes. The retarded Green's function G in frequency domain for the full system (with a similar partitioning scheme as H above) is defined as

$$(E^{+}S - H)G \;=\; I \tag{2.13}$$

where $E^+ = \lim_{\eta \to 0+} E + i\eta$, S is the overlap matrix associated with the non-orthonormal basis with similar partitioning as H and G and I is the identity matrix. Using this definition and the Hamiltonian above, it is possible to write the Green's function of the active region (G_M) as

$$
\begin{aligned}
G_M(E) &= (E^+ S_M - H_M - \Sigma_L(E) - \Sigma_R(E))^{-1} && (2.14)\\
\Sigma_R(E) &= (E^+ S_{MR} - H_{MR})(E^+ S_R - H_R)^{-1}(E^+ S_{MR}^\dagger - H_{MR}^\dagger) && (2.15)\\
\Sigma_L(E) &= (E^+ S_{ML} - H_{ML})(E^+ S_L - H_L)^{-1}(E^+ S_{ML}^\dagger - H_{ML}^\dagger) && (2.16)
\end{aligned}
$$

The shift in energies of the single particle states of the central region is accessible from the real part of $\Sigma_{R/L}(E)$ and the level broadening is obtained from the imaginary part often called $\Gamma_{R/L}(E)$. The one particle density matrix (D_M) for the active region under finite bias is then computed using :

$$
\begin{aligned}
D_M &= \frac{-1}{\pi}\int dE\, Im(G_M(E)) f(E-\mu) \\
&+ \frac{1}{2\pi}\int dE\, G_M(E)\Gamma_R G_M^\dagger [f(E-\mu_R) - f(E-\mu_L)] && (2.17)\\
& && (2.18)
\end{aligned}
$$

where $\Gamma_{R/L}(E) = -2Im(\Sigma_{R/L}(E))$ as mentioned before. The one particle density for the central region is computed from the above density matrix as :

$$
n(r) = \sum_\sigma \sum_{i,k} D^i_{M,\sigma,k} \psi_{i,\sigma}(r)^* \psi_{k,\sigma}(r) \qquad (2.19)
$$

where $\psi_{i,\sigma}(r)$ KS-orbitals defined in previous section obtained from the KS-Hamiltonian

of the active region i.e. of H_M . So the self-consistency procedure involves now starting with a trial guess to construct $H_{M,K-S}$ (Kohn-Sham Hamiltonian of active region), then construct $G_M(E)$ (see Eq.2.14) which also requires knowledge of the bulk electrodes (but they can be computed once and for all). A new density matrix and hence electron density is then computed using Eq.2.17 and 2.18 and then the procedure is repeated until self-convergence. Once converged I vs V characteristics and zero-bias conductance (G) can be obtained as follows:

$$I(V) = \int dE\ T(E)(f(E-\mu_R) - f(E-\mu_L)) \tag{2.20}$$

$$G = \frac{2e^2}{\hbar} T(E) \tag{2.21}$$

where $T(E) = Tr(G_M^{\dagger}\Gamma_R G_M \Gamma_L)$. Further extensive reviews on the method can be found elsewhere [6–8]

2.3 Limitations of the Method

- The explicit lack of dynamic and non-dynamic correlation in the treatment of the electronic structure of the metal-molecule contact by basing the NEGF formalism on DFT. This is mainly due to the single-reference operational framework of the latter and the use of inexact correlation functionals. We shall see later in this thesis for systems involving transition metal complexes in Kondo-resonant devices , correlation and co-operativity in multiple nearly degenerate orbitals becomes necessary.

- Self-interaction error stemming due to usage of LDA and GGA functionals (the hybrid functionals are better in this regard as they include a part of the exact HF exchange which cancels the self-interaction due to Hartree potential) and explicit lack of changing electronic distribution and polarization effects due to the potential. The relaxation

of the many-body states due to the applied electric field is not explicitly taken into account.

- TDDFT used for computing excited state manifold usually predicts lower band-gap which in turn can significantly decrease the potential required to maintain the conducting state thereby over-estimating conductance (see Chapter 3)

- The bulk electrodes in this set-up are treated completely differently than the molecular region. They are considered to be composed of non-interacting electron gas with a Fermi distribution characterized by the respective chemical potentials. Thus correlation effects are explicitly ignored in the electrodes too and hence a theory that holistically treats both the molecule and the leads together is necessary

2.4 Current Constrained variational scheme

Owing to the limitations of the DFT-NEGF method, a transport methodology based on a correlated electronic structure support which employs exact energy functional, treats many-body relaxation due to the electric field explicitly, does not underestimate band-gap and also does not differentiate the system and the electrode but treat them holistically is essential. Much of this thesis is concerned with a work in that direction which we shall elaborate now and in the subsequent chapter.

2.4.1 Deduction of the constraint

The Hamiltonian in Eq.1.12 can be re-arranged as :

$$\hat{H} = \sum_{i<k} \langle i|\hat{h}|k\rangle a_i^\dagger a_k + \sum_{\substack{i<j \\ l<k}} \langle ij|\hat{V}|kl\rangle a_i^\dagger a_j^\dagger a_l a_k \tag{2.22}$$

Using a basis transformation to define new field operators $\hat{\psi}^\dagger(\vec{r})$ and $\hat{\psi}(\vec{r})$ as :

$$\hat{\psi}^\dagger(\vec{r}) = \sum_i \phi_i(\vec{r})^* a_i^\dagger \tag{2.23}$$

$$\hat{\psi}(\vec{r}) = \sum_i \phi_i(\vec{r}) a_i \tag{2.24}$$

$$\{\hat{\psi}^\dagger(\vec{r}), \hat{\psi}^\dagger(\vec{r}')\} = 0 \tag{2.25}$$

$$\{\hat{\psi}(\vec{r}'), \hat{\psi}^\dagger(\vec{r})\} = \delta(\vec{r} - \vec{r}') \tag{2.26}$$

the Hamiltonian in Eq.2.22 can be transformed as :

$$\hat{H} = \int \frac{-\hbar^2}{2m} \nabla^2 \hat{\psi}^\dagger(\vec{r}') \hat{\psi}(\vec{r}) d\vec{r} + \int\int \hat{\psi}^\dagger(\vec{r}) \hat{\psi}^\dagger(\vec{r}') \hat{\psi}(\vec{r}') \hat{\psi}(\vec{r}) \hat{V}(\vec{r}, \vec{r}') d\vec{r} d\vec{r}' \tag{2.27}$$

where the matrix elements of the 1-RDM and 2-RDM and the one-particle density in the position basis are as follows respectively:

$${}^1D(\vec{r}_1, \vec{r}_1') = \langle \Phi | \hat{\psi}^\dagger(\vec{r}_1') \hat{\psi}(\vec{r}_1) | \Phi \rangle \tag{2.28}$$

$${}^2D(\vec{r}_1, \vec{r}_1', \vec{r}_2, \vec{r}_2') = \langle \Phi | \hat{\psi}^\dagger(\vec{r}_1') \hat{\psi}^\dagger(\vec{r}_2') \hat{\psi}(\vec{r}_2) \hat{\psi}(\vec{r}_1) | \Phi \rangle \tag{2.29}$$

$$n(\vec{r}) = \langle \Phi | \hat{\psi}^\dagger(\vec{r}) \hat{\psi}(\vec{r}) | \Phi \rangle \tag{2.30}$$

with the density operator being $\hat{\psi}^\dagger(\vec{r})\hat{\psi}(\vec{r})$. The equation of motion of the density operator in Heisenberg picture is

$$d_t(\hat{\psi}^\dagger(\vec{r}, t)\hat{\psi}(\vec{r}, t)) = \frac{i}{\hbar}[H, \hat{\psi}^\dagger(\vec{r}, t)\hat{\psi}(\vec{r}, t)] \tag{2.31}$$

$$= \frac{\hbar}{2mi} \nabla \cdot (\hat{\psi}^\dagger(\vec{r}, t) \nabla \hat{\psi}(\vec{r}, t) - (\nabla \hat{\psi}^\dagger(\vec{r}, t)) \hat{\psi}(\vec{r}, t)) \tag{2.32}$$

where the Hamiltonian in Eq.2.27 has been used for simplification of the first expression into the second. In analogy with single-particle quantum mechanics, current density operator

(not the field) is:

$$\hat{j}(\vec{r},t) = \frac{\hbar}{2mi}(\hat{\psi}^\dagger(\vec{r},t)\nabla\hat{\psi}(\vec{r},t) - (\nabla\hat{\psi}^\dagger(\vec{r},t))\hat{\psi}(\vec{r},t)) \tag{2.33}$$

With this definition the equation of continuity in Eq.2.32 resembles single-particle quantum mechanics exactly but in terms of operators. The current density vector field then becomes:

$$\vec{J} = \langle\hat{j}(\vec{r},t)\rangle = \frac{\hbar}{2mi}\nabla\langle(\hat{\psi}^\dagger(\vec{r}',t)\hat{\psi}(\vec{r},t) - \hat{\psi}^\dagger(\vec{r},t)\hat{\psi}(\vec{r}',t))\rangle \tag{2.34}$$

$$= \frac{\hbar}{m}\nabla Im({}^1D(\vec{r},\vec{r}')) \tag{2.35}$$

where Eq.2.28 has been used for the 1-RDM. One can also use Eq.2.23 and 2.24 , to recast the above expression in a finite single particle basis as follows:

$$\vec{J} = \frac{\hbar}{m}\nabla Im({}^1D(\vec{r},\vec{r}')) \tag{2.36}$$

$$= \frac{\hbar}{m}\sum_{i,k}\phi_i(\vec{r})^*\nabla\phi_k(\vec{r})Im({}^1D^i_k) \tag{2.37}$$

$$\tag{2.38}$$

where ${}^1D^i_k$ is the spin-traced 1RDM element defined before ${}^1D^i_k = \langle\Phi|\hat{a}^\dagger_i\hat{a}_k|\Phi\rangle$.

Now to define a charge current , we choose the direction of the flux to be a unit vector $\eta = \frac{\sum_k \eta^k e_k}{||\eta||}$ where e_k are the unit vectors along the co-ordinate directions. If we construct a plane in the direction perpendicular to η (the area vector of the plane is parallel to η), then the flux that permeates through the plane projected along the direction of η is

$$I(\eta) = \int_{\eta_\perp}\vec{J}\cdot\eta\ d\eta_\perp$$

$$= \frac{-e\hbar}{m}\sum_{i,k}\int_{\eta_\perp}\phi_i(\vec{r})^*\nabla\phi_k(\vec{r})\cdot\eta\ d\eta_\perp Im({}^1D^i_k) \tag{2.39}$$

Note that the current above is still a function of a one-dimensional spatial co-ordinate η as only the co-ordinates perpendicular to η are integrated out. So the average flux associated with all such planes along the direction of η within co-ordinates $\eta = a$ to $\eta = b$ is

$$
\begin{aligned}
I &= \frac{-e\hbar}{m(b-a)} \sum_{i,k} \int_{\eta=a}^{\eta=b} \int_{\eta_\perp} \phi_i(\vec{r})^* \nabla \phi_k(\vec{r}) \cdot \eta \; d\eta_\perp d\eta \; Im({}^1D_k^i) && (2.40)\\
&= \sum_{i,k} {}^1J_k^i Im({}^1D_k^i) && (2.41)\\
&= Tr({}^1J \; Im({}^1D)) && (2.42)
\end{aligned}
$$

where the matrix elements ${}^1J_k^i = \frac{-e\hbar}{m(b-a)} \int_{\eta=a}^{\eta=b} \int_{\eta_\perp} \phi_i(\vec{r})^* \nabla \phi_k(\vec{r}) \cdot \eta \; d\eta_\perp d\eta$. The current in Eq.2.41, 2.42 is a number only and not a function of any spatial co-ordinates. This is held fixed as a constraint within the optimization scheme to be discussed in the next few sections.

2.4.2 Homomorphic mapping

Since the constraint defined in the previous section

$$
I = Tr({}^1J \; Im({}^1D)) \tag{2.43}
$$

depends on the imaginary part of the 1-RDM, an extension of the scheme elaborated in the previous chapter is essential so as to equip it to handle complex numbers. In this regard, we define a homomorphism $\mathcal{L} : H^{n\times n} \mapsto S^{2n\times 2n}$ wherein H is the space of $n \times n$ Hermitian matrices and $S^{2n\times 2n}$ is the space of $2n \times 2n$ real-symmetric matrices such that

$$
M = Re(M) + iIm(M) \qquad M \, \epsilon \; H^{n\times n} \tag{2.44}
$$

$$
\tag{2.45}
$$

$$\mathcal{L}(M) = \begin{bmatrix} Re(M) & Im(M)^T \\ Im(M) & Re(M) \end{bmatrix}$$

where $\mathcal{L}(M) \ \epsilon \ S^{2n\times 2n}$ as $Re(M)^T = Re(M)$. The map preserves the group properties of complex matrices with respect to addition and multiplication (if commuting) but is only injective. This is because while every Hermitian matrix can be transformed in this fashion into a real symmetric matrix but the converse is not true (real symmetric matrices exists which do not conform to the structure mentioned)

2.4.3 Modified Optimization scheme

With the additional constraint and the mapping defined in previous section , the optimization problem to be used in this thesis becomes :

$$\min_{\mathcal{L}(^2D)} E[\mathcal{L}(^2D)] = \frac{1}{2}\mathrm{Tr}[\mathcal{L}(^2K)\ \mathcal{L}(^2D)] \tag{2.46}$$

$$\text{such that } \mathcal{L}(^2D) \succeq 0 \tag{2.47}$$

$$\mathcal{L}(^2Q) \succeq 0 \tag{2.48}$$

$$\mathcal{L}(^2G) \succeq 0 \tag{2.49}$$

$$\mathrm{Tr}(\mathcal{L}(A_j)\ \mathcal{L}(^2D)) + \mathrm{Tr}(\mathcal{L}(B_j)\ \mathcal{L}(^2Q)) + \mathrm{Tr}(\mathcal{L}(C_j)\ \mathcal{L}(^2G)) = 2b_j.\ \forall j \tag{2.50}$$

$$Tr(\mathcal{L}(^1J)\ \mathcal{L}(^1D)) = 2I \tag{2.51}$$

where as before Eq.2.50 denotes constraints to preserve the linear mapping between the ^2Q,^2D,^2G and also to fix their respective traces. Lot of additional constraints are also introduced to implement the mapping and preserve the structure mentioned in the previous section. By fixing the value of the current in Eq.2.51 , the energy and density matrices so obtained corresponds to a unique minima. This energy is then substracted from the value in absence of the current constraint (I=0) to get the energetic penalty incurred on the system

to maintain the average flux.The modified semidefinite program minimizes the energy over the convex set of two-positive 2-RDMs that support the current I. The optimal 2-RDM supports the current I with the lowest possible energy increase over the energy of a molecule without the current. This response energy is the smallest energy required by the molecule to support the current. Importantly, the steady-state of the molecule with conductivity is a complex superposition of ground and excited states. This complex superposition, driven by the competing goals of energy minimization and current-constraint feasibility, consistently treats both electron transport and electron correlation within a single correlated electronic structure calculation.

2.4.4 Relaxation due to electric field and conversion to potential

To mimic situations in a realistic experimental set-up, one can use the optimization scheme to constrain an average flux over a large chunk (permitted by scaling restrictions)of the device that includes the molecular bridge and some representations of the electrodes. In principle this can be done over the whole-setup including the cell. Now the response energy computed from the model as defined in the previous section will have to be supplied to the system to maintain the flux. Where is this energy coming from ? This is where the role of the potential comes in . The electric field due to the potential at the electrodes changes all the moments of the electron distribution by polarizing the density towards the positive plate. This changes the energy and the population of all the orbitals responsible for contributing to the flux required to cause the polarization. Since we are modeling the event by computing this energetic cost to cause the polarization a priori, this has to be then calibrated against the gain due to the presence of the electric field.

For an electric field $\epsilon = \vec{E}.\eta$ turned in the direction of the current the change in energy of the system can be expanded into a power series as follows:

$$\Delta E_{fld} = \mu_0\epsilon + \frac{1}{2}\alpha_0\epsilon^2 + \frac{1}{6}\gamma_0\epsilon^3 + ... \tag{2.52}$$

where μ_0 is the zero-field dipole moment of the system in the direction η and α_0, γ_0 are the elements of the zero-field polarizabilty and hyperpolarizability tensor. Realistically the only condition needed to be maintain in the circuit for continuous flow is :

$$\Delta E_{fld} \geq \Delta E_{curr} \tag{2.53}$$

with the remaining energy being lost into the surroundings. But for a idealistic dissipationless circuit as is assumed in this work, the minimum energy configuration required to maintain the flow can be obtained by equating the two which gives (after truncation at second order in ϵ):

$$\Delta E_{curr} = \Delta E_{fld} = \mu_0 \epsilon + \frac{1}{2}\alpha_0 \epsilon^2 \tag{2.54}$$

If the electric field used is spatially steady (a reasonable approximation even for AC electric field due to the smallness of the size of the system compared to its wavelength) then the above equation provides a recipe to convert many-body response energy ΔE_{curr} into electric potential(V) that can be maintained at the electrode using the fact $\epsilon = \frac{V}{(b-a)}$. Let L = (b-a) i.e. the length over which the flux is maintained then from Eq.2.54

$$\Delta E_{curr} = \mu_0 \frac{V}{L} + \frac{1}{2}\alpha_0 (\frac{V}{L})^2 \tag{2.55}$$

Since all of the systems used in this thesis is non-polar and symmetric (for asymmetric systems one would have diode-like behavior), the above expression simplifies for V to:

$$V = (\frac{2\Delta E_{curr}}{\alpha_0})^{0.5} L \tag{2.56}$$

This equation Eq.2.56 provides an intuitive and physically motivated justification for the role of potential in transport as the agent which compensates for the re-organization cost incurred on the system by relaxing the energies of the various electronic states which are required to be mixed to maintain a steady flux. The voltage in Eq. (3.2) has trends with re-

spect to changes in length, polarizability, and current that are consistent with expectations. The voltage, for example, increases linearly with length, thereby showing that it is size extensive. A property is size extensive if it scales linearly with system size. Furthermore, as the polarizability molecule increases, the voltage decreases, reflecting the microscopic origin of conductivity in charge polarization. Finally, the energy response of the molecule to the current constraint is computed from solution of the semidefinite program. The energy response can be viewed as arising from a linear but imaginary perturbation in the Hamiltonian due to be applied current. Because the first-order change in energy vanishes, the linear change in the Hamiltonian generates a second-order change in the energy, scaling quadratically in the current. The square root of the energy response in Eq.2.56, therefore, causes the voltage to scale linearly with the current I at low currents.

2.5 References

[1] P. Hohenberg and W. Kohn, Physical Review B **136**, B864 (1964), URL http://link.aps.org/doi/10.1103/PhysRev.136.B864.

[2] W. Kohn and L. J. Sham, Phys. Rev. **140**, A1133 (1965), URL https://link.aps.org/doi/10.1103/PhysRev.140.A1133.

[3] R. Dreizler and E. Gross, *Density Functional Theory: An Approach to the Quantum Many-body Problem* (Berlin, 1990), ISBN 9783540519935, URL https://books.google.com/books?id=1txmQgAACAAJ.

[4] O. Leenaerts, B. Partoens, and F. Peeters, Physical Review B **80**, 245422 (2009).

[5] J. Kohanoff, *Electronic Structure Calculations for Solids and Molecules: Theory and Computational Methods* (Cambridge University Press, 2006), ISBN 9781139453486, URL https://books.google.com/books?id=faRVmAEACAAJ.

[6] J. Taylor, H. Guo, and J. Wang, Phys. Rev. B **63**, 245407 (2001), URL https://link.aps.org/doi/10.1103/PhysRevB.63.245407.

[7] M. Brandbyge, J.-L. Mozos, P. Ordejón, J. Taylor, and K. Stokbro, Phys. Rev. B **65**, 165401 (2002), URL https://link.aps.org/doi/10.1103/PhysRevB.65.165401.

[8] P. S. Damle, A. W. Ghosh, and S. Datta, Phys. Rev. B **64**, 201403 (2001), URL http://link.aps.org/doi/10.1103/PhysRevB.64.201403.

CHAPTER 3

CURRENT-CONSTRAINED VARIATIONAL THEORY - APPLICATIONS IN MOLECULAR ELECTRONICS

- This chapter contains parts of an article that was originally published in the Communications Chemistry. Reproduced with permission from [M.Sajjan and D. A. Mazziotti, *Communications Chemistry*, **1**, 31 (2018)]. Copyright 2018, Springer Nature.
- This chapter contains parts of several articles that are under preparation at the time of writing.

3.1 Introduction

We have developed the theory for current-constrained variational principle in the previous chapter. In the present one, we shall focus on a broad range of applications including length dependance in conductance for polyacenes to effect of electrode substitution in benzenedithiolates to single-molecular pH sensors and analyzing orbital degeneracies in Kondo resonance for a binuclear vanadium complex. Each of the subsequent sections presents the details for each of the aforesaid applications. In all of the calculations mentioned below a finite set of active orbitals were used to correlate in the 2-RDM scheme. Such a method known as complete-active-space 2-RDM calculation [1] has the following steps: (1) initial molecular orbitals are computed from Hartree-Fock calculation, (2) the active orbitals are correlated through a variational 2-RDM calculation wherein the energy is minimized as a functional the 2-RDM subject N-representability constraints [2–4] as well as a current constraint. We employ a necessary set of N-representability constraints known as the two-positivity (or DQG) conditions [3, 5, 6], which constrain three matrix forms of the 2-RDM to be positive semidefinite. (3) the active orbitals are mixed with the remaining (inactive) orbitals to lower the energy, and (4) steps two and three are repeated until convergence. The active-space variational 2-RDM method with 2-positive (DQG) conditions has a polynomial scaling (r_a^6)

as opposed to the exponential scaling e^{r_a} configuration interaction. Once the current is added to the molecule, the 2-RDM becomes Hermitian with its imaginary component containing information about the current. The complex-valued semidefinite program can be solved by mapping it to a real-valued semidefinite program. Just as a complex number can be represented by a real 2x2 matrix, a Hermitian matrix M dimension dxd can be written as a real symmetric matrix S of dimension $2d$x$2d$ [7]

3.2 Length and orientation dependance of conductance - highlighting intrinsic characteristics of oligoacenes

In this section we focus on the length dependance of conductance for the strongly correlated oligoacene molecular wires [1, 8–11] $\{C_{4n+2}H_{2n+4} \mid n \leq 4 \text{ and } n \in \mathbb{Z}^+\}$ along both the longitudinal ($\theta = 0^\circ$) and the transverse axis ($\theta = 90^\circ$) with θ being the angle between the direction of the current imposed and the cylindrical axis of the molecular wire. Calculations were done in STO-6G basis set [12] and the complete set of π orbitals of each of the system were allowed to correlate [1]. An ideal non-invasive electrode setting was assumed. In other words, the molecule is completely decoupled from any leads to see study the influence of its intrinsic characteristics on conductance. Since electrodes in tunnel-coupled geometries are known to make considerable impact, it is needless to say that the conductances produced herein is of theoretical interest only and would only correspond to experimental measurements made in the limit of extremely weak coupling. The study of acene chains is spurred by the importance of polyaromatic hydrocarbons in medicine [13], astrophysics [14], photovoltaics [15, 16], and nano-electronics [17, 18]. Besides even in absence of the current constraint, electronic-structure studies have shown that oligoacenes of moderate length exhibits significant polyradical character which has been efficiently captured using polynomial scaling RDM-methods before [1, 10, 11] unlike wavefunction techniques limited by computational costs.

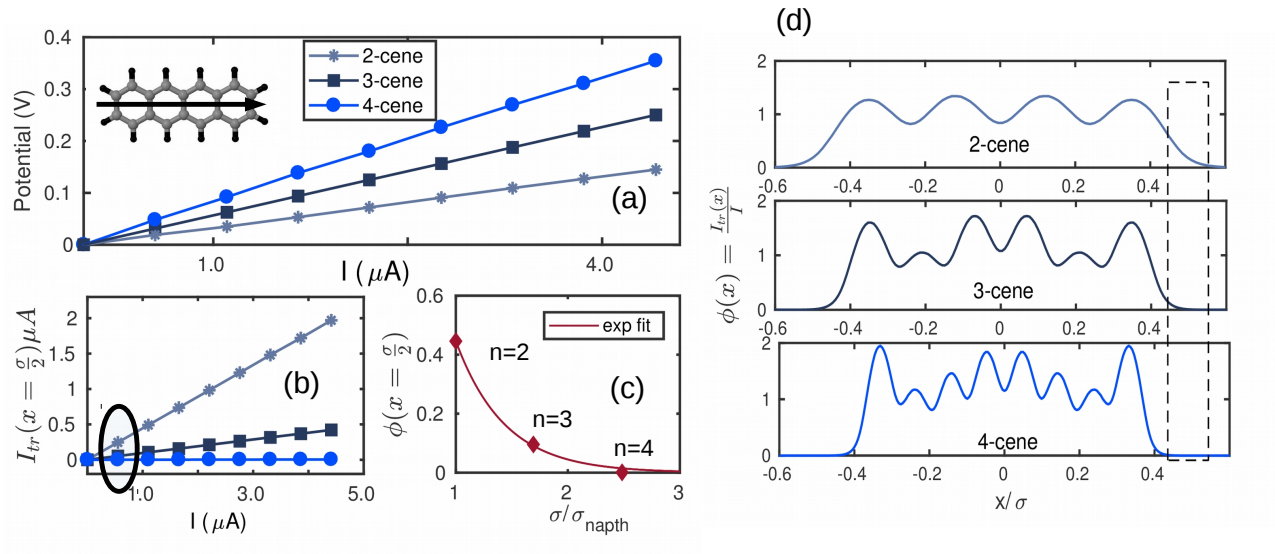

Figure 3.1: (a) The I vs V curve for the oligoacenes till n=4. The 'I' used in this curve is the average flux imposed on the system as discussed in text. The orientation of the flux is along the longitudinal direction of the wires ($\theta = 0$) with the molecular axis taken to be the x-axis. It is illustrated in the inset using tetracene as an example (b) We plot the transmitted section ($I_{tr}(x = \frac{\sigma}{2})$) of the average current which is defined as the flux within a fictitious probe window at the tail end kept at x= $\frac{\sigma}{2}$ (σ is the dispersion in electron density along x for each molecule). It signifies the incoming local current to a lead if an electrode (like an STM tip in experiment) would have been situated at the said location. It is apparent that the transmitted section of the average flux has an explicit exponential dependance on length. (c) We plot $\phi(x = \frac{\sigma}{2}) = \frac{I_{tr}(x=\frac{\sigma}{2})}{I}$ at I = 0.55 μA (highlighted in (b)) against the length of each of the three acenes (n=2,3,4) to expound the exponential decay clearly. The length for each, quantified by the respective dispersion in electron cloud (σ), is expressed as a dimensionless variable normalized to the dispersion for the shortest member i.e. napthalene (n=2) which is $\sigma_{2cene} = 5.218$ Å.The data is fitted to an exponential which provides the parameters A and γ (see text)(d) The local $\phi(x)$ versus the length profile for each of the oligoacenes. The length axis is normalized to the dispersion (σ) of the respective systems. An imaginary probe window centered at $\frac{\sigma}{2}$ illustrates that the area covered by $\phi(x)$ within it declines with increasing length.

In Fig. 3.1 we plot the I vs V curve for the three acenes with average the flux (I) being imposed along the longitudinal direction of the molecular chain (i.e. $\theta = 0$) taken to be the x-axis here. We see an inverse linear dependance of the conductance on length of the molecular wire against the average flux. This is due to the form of the potential V = $\sqrt{\frac{\Delta E}{\alpha_0}}\sigma$. The term $\frac{\Delta E}{\alpha_0}$ is weakly dependant on length due to cancellation of the respective size dependance of the numerator and the denominator, thereby making σ to be the sole contributing factor to the observed trend. To quantify the percentage of the transmitted section of the average flux, we define a variable $\phi(x = \frac{\sigma}{2}) = \frac{I_{tr}(x=\frac{\sigma}{2})}{I}$ wherein $I_{tr}(x = \frac{\sigma}{2})$ is the current collected from an imaginary probe at the tail end of each systems centered at x= $\frac{\sigma}{2}$ (see Fig.3.1(d)) and I is the average current. The symbol $\phi(x = \frac{\sigma}{2})$ explicitly indicates the location of the collection window. The length dependence $(\frac{\sigma}{\sigma_{2cene}})$ of the said quantity is exemplified in Fig. 3.1 (b),(c) which signifies that a local probe like an STM tip in an experiment would experience an exponential drop in the collection of flux when the length of the molecular wire is increased. This is the signature for tunnelling dominated transport which, at the length scale of interest, has been reproduced in many systems [19, 20] including the acenes both experimentally [21] and theoretically [22, 23]. Using this information and the exponential fit in Fig.3.1(c), we further quantify the conductance of these molecular wires (attached to non-interfering electrodes) as follows:

$$\begin{aligned}
\phi(x = \frac{\sigma}{2}) &= A\exp(-\frac{\gamma}{\sigma_{2cene}}\sigma) \\
I_{tr}(x = \frac{\sigma}{2}) &= AG_{avg}(\sigma)\exp(-\frac{\gamma}{\sigma_{2cene}}\sigma)V \qquad \because \quad I = G_{avg}(\sigma)V \\
G(x = \frac{\sigma}{2}) &= G(\sigma)\exp(-\frac{\gamma}{\sigma_{2cene}}\sigma), \qquad G(\sigma) = AG_{avg}(\sigma)
\end{aligned} \tag{3.1}$$

where A (pre-exponential factor) and γ are dimensionless fitting parameters obtained in Fig.3.1(c). The factor $\frac{\gamma}{\sigma_{2cene}}$ is analogous to the Magoga's parameter [24]in our model. We have now also defined two different conductances as follows:

- $G(\sigma)$: This is associated with the average current (see Fig. 3.1a and Eq.3.1) and is due to difference in re-organization energy required to maintain the flux over the whole length of the system for each molecular wire. The re-organization necessitates the mixing the ground and excited states

- $G(x = \frac{\sigma}{2})$: This in addition to the relative differences in the energetic cost mentioned above is also associated with tunelling of charges into the bath. It is quantified here due to the difference in innate tendency of the molecules to spatially distribute the imposed flux towards its tail end (see Fig. 3.1b,c and Eq.3.1).

Length dependencies of these conductances are explored next in Table 3.1.

Table 3.1: Comparison of the various quantities obtained from the model against the length of each system expressed as a dimensionless variable $\frac{\sigma}{\sigma_{2cene}}$ with $\sigma_{2cene} = 5.218$ Å. While A is unitless, the units of $\frac{\gamma}{\sigma_{2cene}}$ is Å^{-1}.
$\text{G}_{avg}(\sigma)$, $G(\sigma) = AG_{avg}(\sigma)$ and $G(x = \frac{\sigma}{2})$ are all expressed in units of G_0 where 1 $G_0 = 2e^2/\hbar$.

Property	2-cene	3-cene	4-cene
σ/σ_{2cene}	1.000	1.692	2.483
A	4.4120	4.4120	4.4120
γ/σ_{2cene}	0.4403	0.4403	0.4403
$\text{G}_{avg}(\sigma)$	0.3756	0.2278	0.1484
$G(\sigma)$	1.6571	1.0050	0.6547
$G(x = \frac{\sigma}{2})$	0.1665	0.0206	0.00218

Several points are apparent from Table 3.1. We see that the exact nature of the length dependences for the two conductances defined above are different. $G(\sigma) \propto (\frac{\sigma}{\sigma_{2cene}})^{-\alpha}$, which from Eq.3.1 makes $G(x = \frac{\sigma}{2}) \propto (\frac{\sigma}{\sigma_{2cene}})^{-\alpha} \exp(-\gamma \frac{\sigma}{\sigma_{2cene}})$ with $\alpha \approx 1$. These dependencies are elaborated below

- Investigating the Magoga's parameter $(\frac{\gamma}{\sigma_{2cene}})$ can lead to important insight into the conduction behavior of $G(x = \frac{\sigma}{2})$. From our calculations and fitting we report in Table 3.1, the value of the said parameter to be 0.4403 Å^{-1} which is in close agreement to experiment[21]. It is further stated in Ref[21], that this parameter is connected to

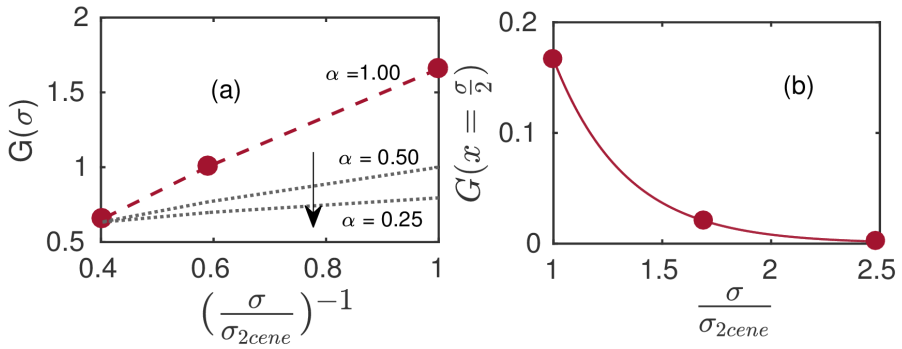

Figure 3.2: (a) The plot of the length dependance of $G(\sigma) = AG_{avg}(\sigma)$ versus $\frac{\sigma}{\sigma_{2cene}}$ for the molecular wires studied. We see that $G(\sigma)$ is proportional to $(\frac{\sigma}{\sigma_{2cene}})^{-1}$ (blue) unlike in Magoga's theory[24]. This is justified using the assertions in Ref[21] wherein it is made explicit that the constant pre-exponential term i.e. $G(\sigma)$ (see Eq.3.1) reduces substantially with enhanced molecule-electrode coupling and is extremely sensitive to the linker too. In our model we use the bare molecular backbone devoid of any electrode or linker, we speculate that an enhanced coupling with the bath with bring down the length scaling to $(\frac{\sigma}{\sigma_{2cene}})^{-\alpha}$ with $\alpha \leq 1$ (black dots) .The arrow indicates reaching the Magoga's limit progressively (b) Length dependence of $G(x = \frac{\sigma}{2})$ is plotted which beyond the re-organization cost and the inverse linear length scaling seen in $G(\sigma)$ has an additional exponential decay associated with tunnelling over the window studied (see Eq.3.1). The decay constant in the exponential (known as Magoga's parameter [24]) is found to be 0.4403 Å^{-1} which is in close agreement with experiment [21]

intrinsic characteristics of the system and is nearly independent of the electrode setup even though very weakly dependant on the linker used (see Fig.8(A) in Ref[21]). This explains the close agreement with our model wherein the effect of the electrode is ignored. Also it resembles more closely the value for the monothiol acene junctions (reported in Ref[21] to be 0.5 Å^{-1}) than to dithiol junctions (reported in Ref[21] to be 0.2 Å^{-1}) as is expected from calculations on a bare molecular backbone devoid of linking substituents. This also further explicates that the exponential part of $G(x = \frac{\sigma}{2})$ will not change much by changing the bath and the linker.

- As mentioned before (see Eq.3.1) since the the pre-exponential factor $G(\sigma)$ is itself length sensitive ($\propto (\frac{\sigma}{\sigma_{2cene}})^{-1}$), the combined length dependence of $G(x = \frac{\sigma}{2})$ is $(\frac{\sigma}{\sigma_{2cene}})^{-1} \exp(-\gamma \frac{\sigma}{\sigma_{2cene}})$ unlike in Magoga's theory wherein it is a single-exponential decay[24]. This is justifiable from the analysis in Ref[21] wherein it is stated that the pre-exponential factor is decreased strongly due to electrodes with high work-function and also for good linkers (see Fig.8(B) in Ref[21]) both of which are absent in our model as it focuses on the intrinsic characteristic of the molecule alone. We speculate as indicated in Fig.3.2a that a stronger coupling of the system to the electrode should not only decrease the value of $G(\sigma)$ for each wire but also reduce the length scaling (as longer acenes have high DOS which should provide more channels for coupling) thereby making the length dependence reach Magoga's limit progressively (i.e. $G(\sigma) \propto (\frac{\sigma}{\sigma_{2cene}})^{-\alpha}$ with $\alpha \leq 1$). In that limit the length dependence of $G(x = \frac{\sigma}{2})$ would therefore be approximately a pure exponential.

To illustrate the orientation dependance of conductance in Fig.3.2(a) we plot the I vs V curves for the oligoacenes in a transverse orientation ($\theta = 90$) with the direction of the flux being taken to be the y-axis. This is illustrated in the inset using tetracene again. Unlike in the previous case when their respective lengths have dominated the trend in their conductance described above both at the level of average flux as well as its transmitted section, we see that in the new orientation away from the molecular axis, the oligoacenes

presents completely reversed trend in their conductances commensurate with the electronic structure of the molecules which entails a decreasing band gap. An expression analogous to Eq.2.1 would indicate that the conductance for the acenes in this new orientation is controlled entirely by the $G(\sigma)$ term which for the same σ (dispersion in electron density along y) as is the case here is controlled by the $\sqrt{\frac{\Delta E}{\alpha_0}}$ term in the potential. To maintain a flux across the same length, higher acenes incurs a less re-organization cost (less ΔE) due increased quasi-degeneracy of the π orbitals which leads to high density of many-body states. This also makes the system more polarizable and enhances the response to electric field augmenting the α_0 term. In Fig.3.2 (b) as before we plot the transmitted section of the current ($I_{tr}(y = \frac{\sigma}{2})$ near the zero-bias limit at I = 0.55 μA and see that it is almost sub-linearly increasing (for n=2 to 3) and then begin to saturate unlike in the previous case where we had a continuous exponential drop. This can be explained by noting that even though the number of single-particle modes which supports the flux increases down the series, the modes are less transmissive over a longer length when considered in the longitudinal orientation unlike in the shorter transverse orientation wherein the spatial gap being same only their enhanced number makes the only difference. This reversal in conductance (see Fig.3.2(c)) trend due to changing orientation has been verified in amminoacenes [25] and more recently on the molecular backbone directly[26] even though the exact transport axis in the latter is slightly tilted away from the molecular plane unlike in our calculations.

In conclusion, through our model we study the length dependence of conductance in oligoacenes by defining two different measures of conductances namely $G(\sigma)$ and $G(x = \frac{\sigma}{2})$. While $G(\sigma)$ is associated with the re-organization cost required to maintain the total average flux over the system, $G(x = \frac{\sigma}{2})$ in addition to this energetic cost is also sensitive to the differences in the innate tendency of the molecular wires to support flux towards its tail end so as to facilitate tunelling into the electrodes. This kind of analysis allows us to peel the effect of length on these individual conductances which is $(\frac{\sigma}{\sigma_{2cene}})^{-1}$ for the $G(\sigma)$ (see Fig 3.2(a) and Eq.2.1)due to the σ term in the potential and $(\frac{\sigma}{\sigma_{2cene}})^{-1} \exp(-\gamma \frac{\sigma}{\sigma_{2cene}})$ for the

$G(x = \frac{\sigma}{2})$ (see Fig 3.2(b) and Eq.2.1) due to additional sensitivity to charge distribution on the backbone over and above the dependances in $G(\sigma)$. Even though previous theories have focused on $G(x = \frac{\sigma}{2})$, the analysis of $G(\sigma)$ has been eluded and to the best of our knowledge is the first of its kind. We also discuss the parameters in the two conductances and report that the Magoga's constant for the oligoacene series is 0.4403 Å^{-1} which being insensitive to external coupling is in close to experimental values[21]. We then justify in what limit the two expressions above based on intrinsic properties of the molecule would collapse (see Fig.3.2) to the Magoga's formula [24]. Thereafter we reproduce the experimentally verified reversal in conductance trend due to switching in orientation of transport axis in the oligoacene family. In the latter case the length being the same, the sole contributing factor becomes the density of modes thereby lowering the re-organization cost for higher acenes.

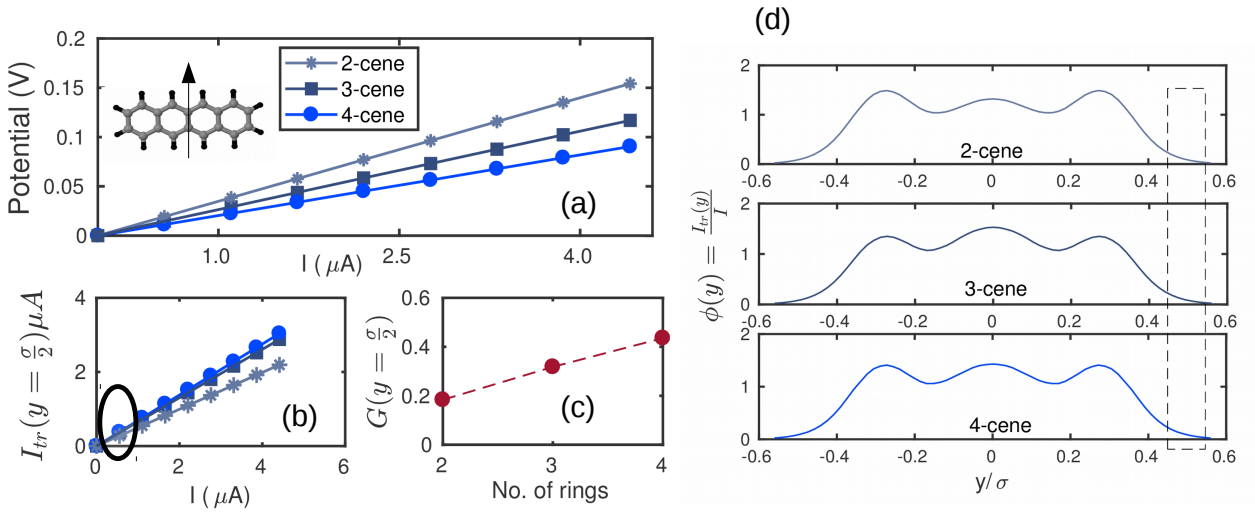

Figure 3.3: (a) The I vs V curve for the oligoacenes till n=4. The 'I' used in this curve is the average flux imposed on the system as discussed in text. The orientation of the flux is along the transverse direction of the wires ($\theta = 90$) with the transport axis taken to be the y-axis. It is illustrated in the inset using tetracene as an example (b) We plot the transmitted section ($I_{tr}(y = \frac{\sigma}{2})$) of the average current which is defined as the flux within a fictitious probe window at the tail end kept at y= $\frac{\sigma}{2}$ (σ is the dispersion in electron density for each molecule along y). It is apparent that the transmitted section of the average flux increases sub-linearly from n=2 to 3 and then saturates. (c) We plot $G(\sigma)$ (analogue of Fig. 3.2) against the number of rings for the three acenes (n=2,3,4) to expound linear rise. (d) The local $\phi(y)$ versus the length profile for each of the oligoacenes. The length axis is normalized to the dispersion (σ) along y of the respective systems. An imaginary probe window centered at $\frac{\sigma}{2}$ illustrates that the area covered by $\phi(y)$ within it remains nearly the similar in this orientation.

3.3 Effect of electrode substitution in benzene-dithiolates and chemical substitution on benzenediamines

In this section, the current-constrained variational principle, implemented in the variational 2-RDM method, is applied to computing the conductance of the 1,4-benzenedithiol molecule, shown schematically in Fig.3.4, which has been used extensively to benchmark both experimental [27–31] and theoretical studies [32–39]. Due to the small size of the molecule and the atomistic molecule-electrode contact typically used in an experiment, a single atom lead is a reasonable, first-order approximation to the junction between the lead and the molecule. While the average current across the entire molecule and lead was constrained within the variational calculation, we report the average current confined to the lead, which is the location where the current is experimentally measured. Computations with the variational 2-RDM method [5, 6, 40] were performed in a finite basis set which is 6-311G* for sulfur, 6-311G for carbon and hydrogen and LANL2TZ (with ECP) for the metals. An active space of 15 orbitals with 16 electrons [15o,16e] of π symmetry was used for the calculations. The length of the molecule was set to the dispersion of r in the direction of the molecule at zero field which measures the length of the molecule by the extent of its electron cloud. At finite field the dispersion (length) of the molecule was kept fixed to its zero-field value by additional constraint in the semidefinite program. This constraint, however, was not found to affect the result significant, and in most cases it can be neglected.

Fig.3.5(a) shows the I-V curves from a range of theoretical methods [32, 34, 35] and experiment [27] as well as from the variational 2-RDM method (labeled 2-RDM). NEGF-DFT results [34, 35] are shown from a range of density functionals including PZ, B3LYP, and M06. All three of these methods yield currents that are 1 to 2 orders of magnitude larger than those from the experiment. It is well-known that DFT with NEGF tends to overpredict the conductance by a significant amount, potentially orders of magnitude [34, 35, 43–45]. The over prediction has been attributed to several factors including the energetic positioning

Figure 3.4: (a) The 1,4-benzenedithiol molecule, connected to gold-atom leads, has been used extensively to benchmark both experimental [27–31, 41] and theoretical studies [32, 34, 35]. (b) The same molecule with the electrode substituted with nickel atoms

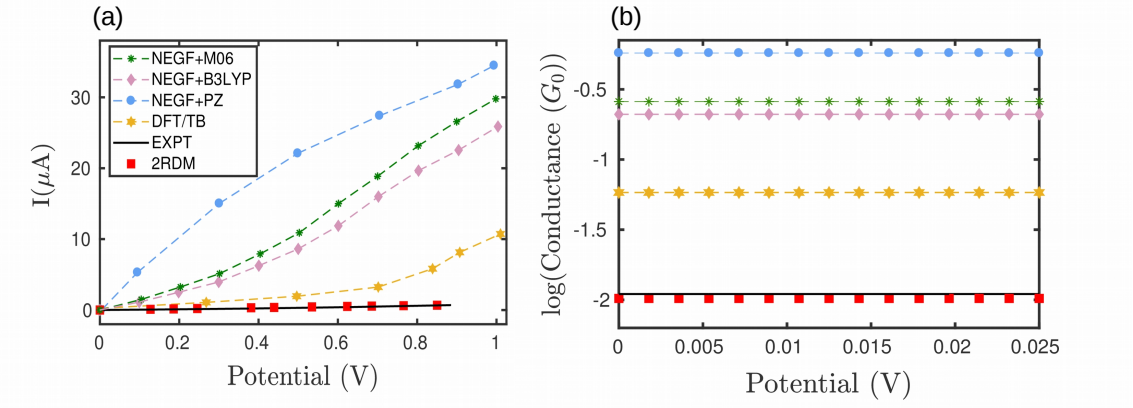

Figure 3.5: (a) Comparison of I-V curves from a range of theoretical methods and experiments for BDT-Au. The I-V curve from the constrained-current variational 2-RDM method (labeled 2-RDM) is compared with the I-V curves from a range of theoretical methods [32, 34, 35] and experiment [27]. Many of the previous theoretical calculations yield currents that are 1 to 2 orders of magnitude larger than those from the experiment [27]; the current-constrained 2-RDM theory, in contrast, yields currents that match the experimental results [28–30] for the range of available voltages. (b) While the 2-RDM and experimental currents appear to be zero in a relative to previous predictions, the graph in b displays the base-10 log of the conductance as a function of the voltage, showing that the currents from the 2-RDM method are nonzero and essentially equivalent to those from the experiment.

Table 3.2: Comparison of the computed and measured conductances from several theories and experiments with the conductance from the current-constrained variational 2-RDM method for BDT-Au. While previous theoretical studies overpredict the conductance as discussed above, both the 2-RDM method and the majority of experiments predict a conductance of $\approx 0.011\ G_0$ for 1,4-benzenedithiol with gold leads where $1\ G_0 = 2e^2/\hbar$.

Source	Conductance(G_0)
DFT/TightBinding[32]	0.058
NEGF-DFT(PZ)[34]	0.57
NEGF-DFT(MO6)[35]	0.25
NEGF-DFT(B3LYP)[35]	0.21
Expt[27]	0.011
Expt[42]	0.01-0.015
Expt[28]	0.01
Expt[29]	0.01
Expt[31]	0.01-0.08
2RDM(present)	0.0102

of the Kohn-Sham orbitals. The current-constrained 2-RDM method, in contrast, yields currents that match the experimental results for the range of available voltages. While the 2-RDM and experimental currents appear to be zero in Figs.3.5(a) relative to previous predictions, Fig.3.5(b) displays the base-10 log of the conductance as a function of the voltage, showing that the currents from the 2-RDM method are nonzero and essentially equivalent to those from the experiment. Table 1 compares the computed and measured conductances from several theories and experiments with the conductance from the current-constrained variational 2-RDM method. While previous theoretical studies overpredict the conductance as discussed above, both the 2-RDM method and the majority of experiments predict a conductance of 0.01 for 1,4-benzenedithiol with gold leads.

Chemical substitution has a large role in controlling conductivity in molecular circuit design. Molecular changes can be made not only to the molecule but also to the linkers and the leads. First we explore the effect of substituting the gold-atom lead with a nickel-atom lead in 1,4-benzenedithiol. Fig.3.6 shows the I-V curves of 1,4-benzenedithiol with the gold and nickel leads. Benzenedithiol with the nickel lead is predicted by the 2-RDM method to have approximately twice the conductance of the molecule with the gold leads. This result

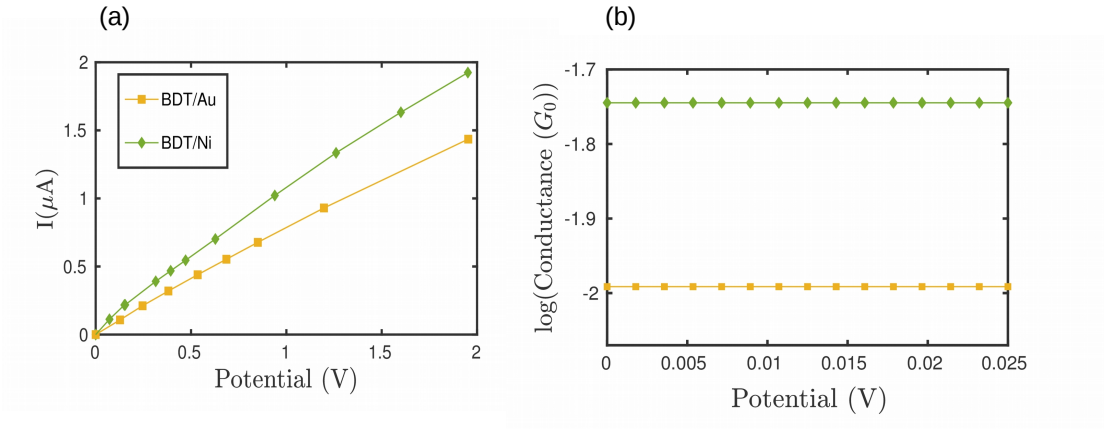

Figure 3.6: a The I-V curves of 1,4-benzenedithiol with the gold and nickel leads are compared. b, The base-10 log of conductance versus V curves of 1,4-benzenedithiol with the gold and nickel leads are compared. Benzenedithiol with the nickel lead is predicted by the 2-RDM method to have approximately twice the conductance of the molecule with the gold leads, which is consistent with recent experimental observations [46].

is consistent with a recent experiment which found that the conductivity was enhanced by a factor of two [46].

Having elucidated the characteristics for electrode replacement in the dithiolates, we now proceed to explicate the effect of linking groups and chemical substitutions on the molecular backbone. In recent years apart from thiols (SH), amine linkers (NH_2) have been used extensively [42, 44] as they produce low dispersion in conductance measurements. In 2007, benzene molecules flanked by NH_2 linkers were used to study the effect of replacement of chemical functionalities and substituents on the molecular framework [47]. A range of electron-withdrawing groups(EWG) like F, Br, I, CN, NO_2 and electron-donating (EDG) groups like NH_2,CH_3,OCH_3 were used to alter single-molecular conductance relative to the unsubstituted variety. In Fig.3.7, we plot the I vs V curves for 2 EWG (F, CN) from the list and 2 EDG too (CH_3,NH_2) in addition to bare 1,4-benzenediamine (BDA). A single atom Au electrode as before was used for the study. The basis set and the active space involved is the same as for the dithiolates with 6-311G being used for the substituting moeities. We not only see that the single-molecular conductance for BDA being lesser than the corresponding

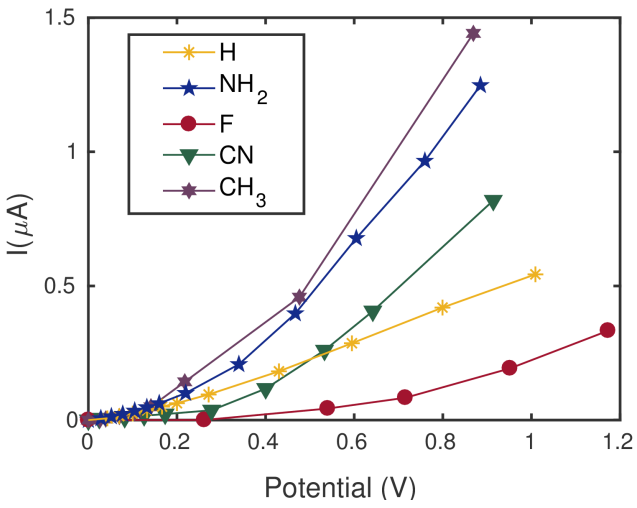

Figure 3.7: I vs V plot for the comparison of substituent effects in BDA/Au junction. It is clear that EWG decreases the zero-bias conductance while the reverse happens with EDG relative to the unsubstituted specie as reported experimentally [47]. All substituents used are tetra-substituted on the molecular backbone

dithiolate (see Table 3.2 and 3.3) but EWG (EDG) tends to decrease (increase) the conductance as reported experimentally [47]. Intuitively, more electronegative substituents like EWG withdraws charge density from the junction and also lowers the energies of the frontier single-particle modes of the system which in turn hinders coupling with the Fermi-level of the electrodes and reduces tunelling of charges away from the system. The reverse happens with EDGs. Table 3.3 highlights the respective single-molecular conductances obtained from our calculations when compared against the experimental results. Even though the exact numerical values varies yet we see our results captures the accurate trend as well as the order of magnitude in most cases. The geometries used for all computations were the same as that used for the dithiolates for comparison. However it is reported that for BDA there are several competing conformations can participate in the process [44] which might explain the numerical discordance.

Thus we see that application of the theory to the 1,4-benzenedithiol molecule with gold-atom leads improves the conductances from existing theories by 1-2 orders of mag-

Table 3.3: Comparison of the computed and measured conductances from 2-RDM theory and experiments in units of G_0 for different substituents (all tetrasubstituted) in BDA/Au junction. A qualifier of mono/di/tri would indicate that the mono/di and trisubstituted variety has been used in the experiment.

System	Source	Conductance(G_0)
H	Expt[44, 47]	0.0064
	2RDM	0.0042
NH_2	Expt	-
	2RDM	0.0051
CN	Expt[47](mono)	0.0059
	2RDM	0.0023
F	Expt[47]	0.0052
	2RDM	0.0015
CH_3	Expt[47]	0.0082
	2RDM	0.0047

nitude [32, 34, 35], matching experimentally measured conductances of 0.01 G_0 [27–30] as well qualitatively and quantitatively predicts the right order of conductance on electrode replacement from gold to nickel. Furthermore our theory is able to correctly capture the qualitative trend in substitution of the linker from SH to NH_2 as in BDA and replacement of electronic moeities within the specie too.

3.4 Role of Correlation (Orbital Degeneracies) in Kondo Resonance

Several decades after its initial experimental discovery [48], Jun Kondo in 1964 using third-order perturbative arguments showed a logarithmic divergence in resistivity for metallic conductors with magnetic impurities ascribed to spin-pairing below a threshold temperature[49]. However, it was realized subsequently that the consequences of the effect would be reversed in tunnel-coupled geometry [50–52] commonly known as 'Kondo resonance'. Understanding the effect of quantum entanglement in such resonance is of significant importance both fundamentally and technologically in developing new materials for molecular electronics and spintronics. Over the past decade, Kondo resonance has been amply verified in systems like quantum dot heterostructures [53], surface adatoms [54, 55] and even in transition metal complexes explicitly devoid of magnetic centers [56–60]. In the more exotic varieties, apart from the manipulation of local spin, orbital or charge degeneracies have been exploited experimentally as an additional degree of freedom to augment the effect in engineered systems[61–67].However theoretical attention to the latter prospect especially in real molecular examples is largely unexplored beyond the understanding provided by extensions of conventional impurity paradigms [68–70].

In this contribution, we explicate the source and the role of a many-body entanglement in a conducting state, arising due to such orbital degeneracies (leading to non-vanishing contributions of multiple reference configurations), on Kondo resonance using recently developed reduced density matrix (RDM) based transport[71] and excited states[72] methods. We illustrate our stand on the mimic of a binuclear complex (see Fig.1.) and its positively charged state known to display remarkable Kondo resonance[57] and point to innate degeneracy in the orbital spectrum apart from the usual spin degeneracies which can be tuned in subsequent studies by manipulating the coupling to the reservoirs[66]. We thereby describe the results using appropriate many-body measures and analyze the influence of such

degeneracies on the enhanced Kondo signature of the system. Even though some effort has been spared in recent years[73], it is clear that practical implementation of most transport theories reliant on DFT based electronic structure method would fail to acknowledge such inherently strong multi-reference correlation effects due to the usage inaccurate exchange correlation functional unlike RDM which has been known to tackle such effects with significant accuracy[10, 74–76] .

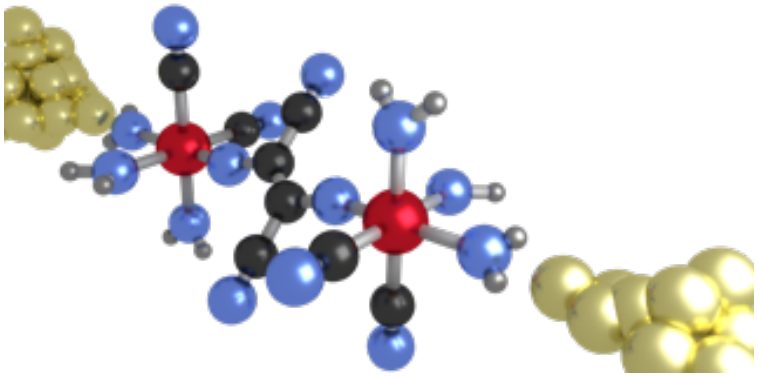

Figure 3.8: The binuclear complex V_2/V_2^+ [57] used in the present study capped with Au atoms (shown in gold). The vanadium centers are in red, nitrogen atoms in blue, carbon atoms in black, hydrogen atoms in grey. Unlike in [57], the nitrogens of the trazacyclononane moeties are replaced by NH_2 groups but the fumaronitrile bridge (μ-C_4N_4), the co-ordination sites of the vanadiums and the identity of all the ligating atoms are kept intact.

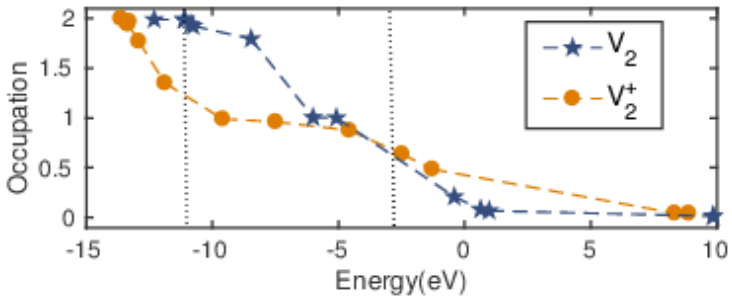

Figure 3.9: The Fermi surface for the binuclear spin-singlet complex V_2 (blue) and the corresponding spin-doublet V_2^+(maroon) formed post charging. For V_2, the orbital degeneracy is 2 (diradial) where each of the SONOs(NO with occupancy 1, see Fig.3.10) can house an electron with opposite spin (anti-ferromagnetically coupled) to create an overall singlet. For V_2^+, the plateau like appearance at the center indicates a number of SONOs referring to strong multi-reference effects due to orbital degeneracies.

We use for all computations a very close mimic of the molecule studied in Ref[57]. To keep the ligating atoms on the vanadium centers same, only the N units of the triazacyclononane moieties are replaced by NH_2 groups in the mimic (see Fig.3.8) for computational convenience. The geometrical parameters are obtained from the crystal structure described in Ref[77] The calculations also involve two Au atomic centers placed $2.0\mathring{A}$ apart from the axial NH_2 groups as representations of the electrode in the weak-coupling limit which is known to be the Kondo-regime [53, 57]. The basis set used is LANL2Dz for the metals with effective core potential(ECP) and 6-311g for the N,C and H. The neutral specie (henceforth referred as V_2 as in Ref[57]) which has a spin-singlet ground state is treated using an active-space formulation [1] of the aforementioned semi-definite scheme in PySCF in a space of [20e, 16o] whereas the cationic form (henceforth referred as V_2^+ as in Ref[57]) possessing a spin-doublet ground state is treated in an active space of [21e, 16o]. The active orbitals for both the systems involves energetically frontier states of π and σ symmetry involving all the metal centers and the ligating atoms. The excited state computations for each specie were done using an algorithm under development by one of the co-authors[72].To compute the zero-field polarizabilities for the ground states, WF-CASSCF in GAMESS electronic structure package was used with an active space of [18e,14o] for the neutral form and [19e,14o] for the cationic form

The electronic structure calculation on the neutral and cationic species using the current constrained variational scheme above in absence of an average flux yields an ionization energy of 2.5062 eV for the discharging of neutral V_2 which is roughly the strength of the anti-ferromagnetic coupling between the two unlike spins in the corresponding spin singlet (S = 0) configuration of the latter specie . An uncorrelated mean field description of the electronic structure of V_2 would correspond to a single-Slater determinantal ansatz with double occupancy until the highest occupied orbital.

To investigate whether the description holds, we also plot the occupancies and the energies of the natural orbitals (NOs), which are eigenmodes of the 1-RDM obtained from

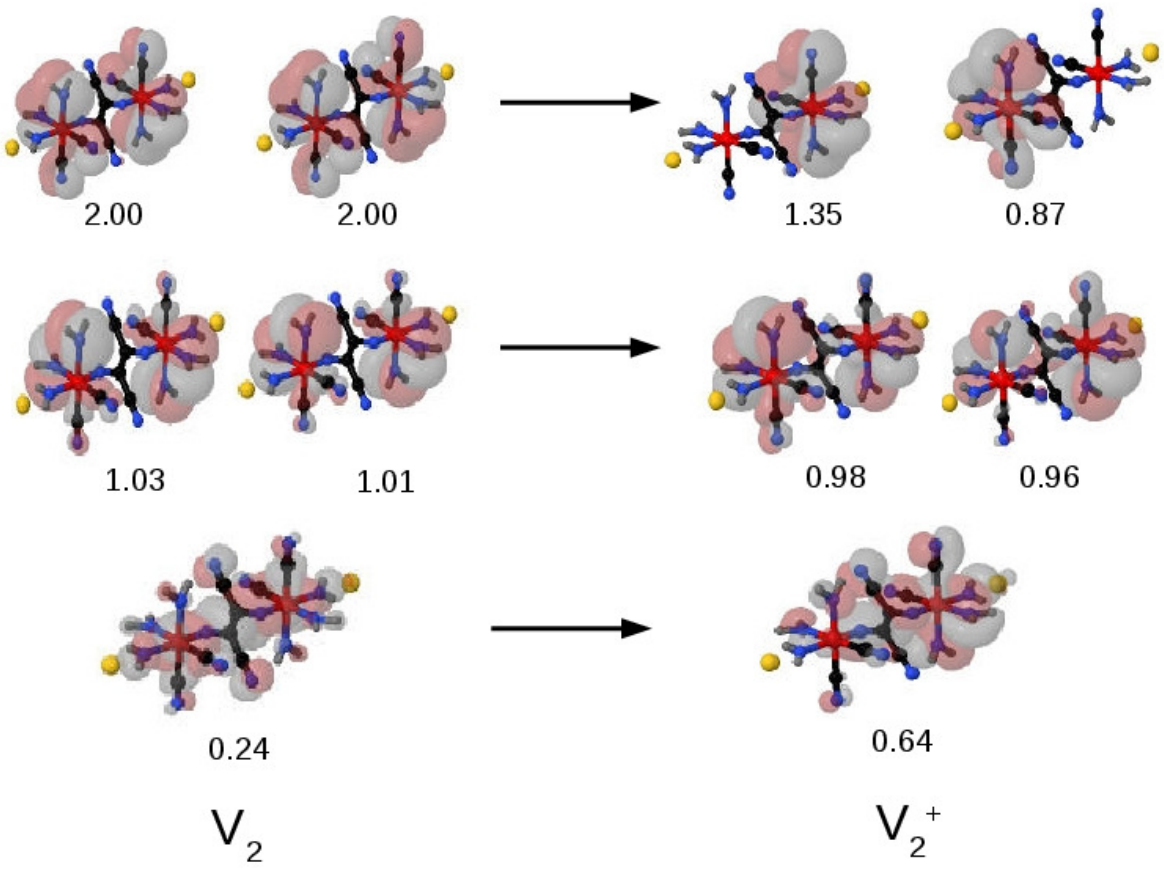

Figure 3.10: The electron distribution for the NOs of V_2 (left) that has highest overlap with those of V_2^+ (right) post oxidation plotted with a cutoff grid of 0.005. The occupation numbers for each NO is listed below for both the species. We see that V_2 behaves as a diradical with two phase-flipped SONOs (middle-left) of π symmetry shared primarily between the d_{xy} of the vanadium centers and the CN (eq), NH_2(eq) ligands. However V_2^+ has a clear multi-radical character (right) with a number of SONOs as seen in Fig.3.9. Also the SONOs of V_2 continues to enjoy single-occupancy even in V_2^+ (middle-right) but previously filled orbitals in V_2 (top-left) have been depleted extensively (top-right). Since the charge distribution on the latter NOs were primarily on CN (eq), NH_2(eq), it is unsurprising to see the Mulliken charges of these ligands have increased (see Table I). Also nearly empty orbital on V_2 (bottom-left) enjoys non-negligeble occupancy in V_2^+ (bottom-right) with charge distribution on the bridging ligand (μ-C_4N_4) explaining the slight decrement in its Mulliken charge.(see Table I)

.

the optimization scheme, in Fig.3.9(blue) and see that the specie displays a clear diradical character involving two quasi-degenerate singly-occupied orbitals (SONOs), each of which is equally likely to hold a spin-up or spin-down electron. For the cationic V_2^+, the ground state is a spin doublet ($S = \frac{1}{2}$). The occupation spectrum plotted in Fig 3.9(orange) shows significant polyradical character with a number of NOs displaying non-negligible population unlike the mean field picture which simply accounts for one singly occupied level. Such orbital degeneracies have been reported elsewhere in lanthanide impurities too [78].

Table 3.4: Comparison of the changes in Mulliken charges for the various moeities in V_2/V_2^+ prior and post redox event

Groups/Atoms	Mulliken charges		Δ
	V_2	V_2^+	
V(1)	1.26241	1.32438	0.06197
V(2)	1.26265	1.25651	-0.00614
μ-C_4N_4	-0.42458	-0.61902	-0.19444
4CN(eq)	-1.68628	-1.42772	0.25856
$4NH_2$(eq)	-0.74324	0.04722	0.79046
$2NH_2$(ax)	-1.11382	-1.12828	-0.01446
2Au	1.44282	1.54690	0.10408

Ligand non-innocence in redox events have been studied and reported before in numerous examples [74, 79] using the variational scheme being discussed here. To describe the changing spatial distribution of the electron density within the molecular framework during the oxidation of V_2 to V_2^+, in Table I we display the absolute and relative Mulliken charges of the various ligating centers and the metal atoms. We notice a primary depletion of negative charges from the equatorial CN and NH_2 post oxidation. To analyze this, the contour plots for the electronic distribution of the NOs of V_2 and those with highest overlap in V_2^+ after oxidation are shown in Fig 3.10. While we see that the SONOs of V_2 indicated in Fig.3.10 are of π symmetry with density being shared between the d_{xy} orbitals of vanadium centers and the equatorial CN and NH_2 ligands mainly (middle-left in Fig.3.10), but these NOs continue to enjoy single occupancy even in V_2^+ (middle-right in Fig.3.10). The ones depleted had a preponderance of charge density on the equatorial CN and NH_2 ligands prior

to oxidation (see top-left and right panel of Fig.3.10) which corroborates why the latter ligands have selectively bled.A slight increase in occupancy post oxidation in the NO with appreciable charge density on μ-C_4N_4 (bottom-left and right panel Fig.3.10) also justifies the plummeting of its Mulliken charge too.

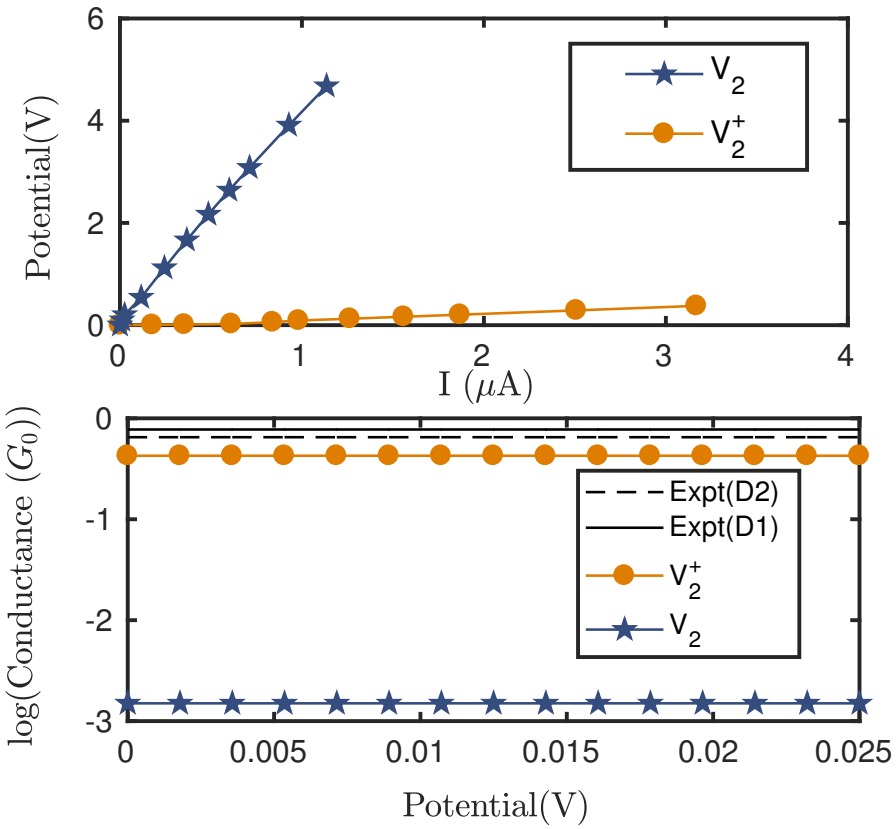

Figure 3.11: (a) The I vs V profile for V_2 (blue) and V_2^+(orange) computed from the current constrained variational theory.We see that V_2^+ requires a much lesser potential to support the similar a transmitted flux on the capping Au atoms unlike V_2. (b) The logarithm (base-10) of the zero-bias conductances for V_2 (blue) and V_2^+ (orange). The results for V_2^+ are in good agreement with experimental results (shown in black for two trials D1, D2 in Ref[57]). We see that a steep discontinuous order of magnitude increase in conductance due to single electron discharging creating the spin-doublet V_2^+ at negative gate biases. This corroborates the observations in the experimental set-up used for the SET and provides an indication of Kondo resonance.

In Ref[57], the said binuclear complexes has been used in an SET to study the electronic conduction behavior of the neutral V_2 and the cationic V_2^+ form. Electrostatic gating using

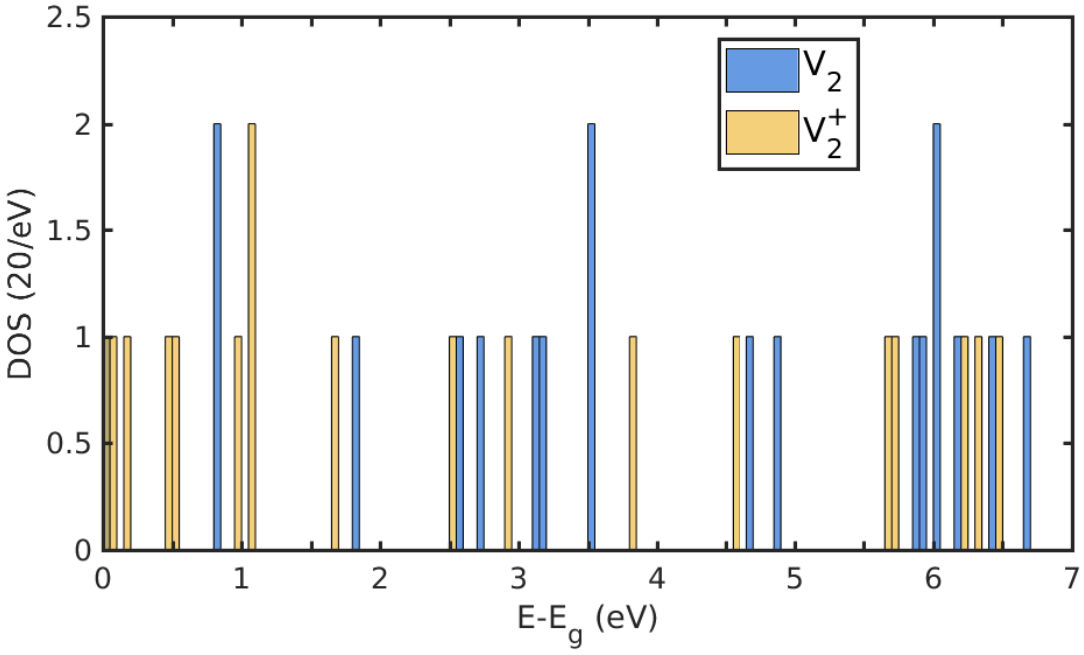

Figure 3.12: The DOS of the excitation manifold (without spin degeneracies) for V_2 and V_2^+ computed from a recently developed algorithm from one of the co-authors. The unit indicates 20 states per eV of energy. The ground state for V_2 and V_2^+ are spin-singlets and doublet respectively. We see that near the ground state (peaks at zero) there are far more number of many-body states in V_2^+ than in V_2 which enables more channels to be available to couple with the many-body states of the bulk electrodes leading to the Kondo-resonance and also decreases the energetic cost of the conducting state produced enhancing the zero-bias conductance

the Al_2O_3 layer allows one to toggle reversibly between the two charged and spin states, with the positive gate potential disfavoring the cationic form (enhances the ionization energy computed before) relative to the neutral one whereas negative gate potential stabilizing the discharging of V_2 to V_2^+ by lowering the ground state of the positively charged specie. At the charge degeneracy point the respective energies of the two species would be nearly equal. It is seen in the experiment that the zero-bias (source-drain) conductance of V_2^+ is significantly higher than the neutral form (see Fig 1a, 1b in Ref[57]. In Fig 3.11(a) we plot the I vs V profile for both the species from the current-constrained variational principle discussed and see that not only our results are qualitatively consistent with the experiment, but the numerical magnitude of the zero-bias conductance reported for V_2^+ is in good agreement too (Fig 3.11(b)). Such a discontinuous jump in conductance associated with an spin-doublet configuration through single electron discharging from a singlet precursor is an indicator of Kondo resonance in the odd electron specie.

Conventional explanation for such discontinuous conductance switching is by single-level Anderson impurity model [57, 80] wherein the stable spin doublet formed (here V_2^+), opens up a single half-filled channel which can overlap with the orbitals of either electrode and establish an anti-ferromagnetic coupling with the itinerant spins of the host near Fermi-level leading to strong resonant condition (Kondo-resonance). Theorized as the global Kondo singlet ground state formed between the molecule and the host, it can exhibit spin-flip scattering which explains the conduction behavior. For a correlated case like this with additional orbital degeneracies, the effect can be magnified as can be seen from Fig.3.9 and 3.10 wherein we see that a large array of SONOs exist for V_2^+ with appreciable electron density towards the Au terminus (Fig.3.10) thereby enabling them to participate in coupling with unlike spins of the bulk electrodes. Even for V_2, unlike in the single-state model, we have two quasi-degenerate SONOs (Fig.3.9) with density distribution on either half of the molecule (Fig.3.10) housing electrons with opposite spin and is internally spin locked due to this anti-ferromagnetic coupling. In addition, high ionization energy for V_2 (computed

before) also makes it impossible to flip the charge state at positive gate bias explaining the blockade.

However as is clear from the electronic structure of V_2 and V_2^+, the very presence of orbital degeneracies presents important multi-reference effects especially in the latter and hence we would like to establish conclusions through many-body computations. In Fig.3.12 we plot the DOS of the many-body states in absence of spin degeneracies obtained from a novel algorithm designed using the ground state guess from a variational 2RDM calculation by one of the co-authors [72]. We see that the DOS for the many-body states of V_2^+ near the ground state are relatively much higher which indicates that there are more available multi-party channels formed by the coupling of the Au orbitals and the substrate (bare-complex) in its charged spin-doublet form near the Fermi-level of the bulk host. These channels are thereby available to couple with the many-body charge and spin states of the bulk electrodes leading to resonant transport (Kondo resonance in the correlated picture) and an ease in the formation of the global Kondo singlet. Alternatively, the thick manifold of states also explains why the response energy obtained in the current-constrained variational calculation for successive values of average flux (see Table S1) is less for V_2^+ by two-orders of magnitude as formation of a non-stationary state consistent with the flux is less costly.The high Kondo temperature (30 mK) recorded for the complex [57] might be due to the fact that the resonance would be immune to thermal decoherence due to such high many-body DOS owing to orbital degeneracies upto temperatures higher than usually seen.

In conclusion, in the present report we have analyzed the electronic structure of a bi-nuclear complex used for an SET study [57] using correlated electronic structure method like variational 2-RDM and report important multi-reference effects and ligand centered oxidation. We also do a zero-bias conductance calculation using a recently developed current constrained density matrix method and found an excellent qualitative and quantitative agreement between the computation and the experiment with regard to conductance jump on discharging V_2 and we explain the effect through appropriate many-body evaluations of

the excited state manifold unlike the single-level Anderson impurity model which is conventionally employed. Even though outside the scope of the present work, we can speculate about the other signatures of Kondo physics like effect of external parameters like temperature and magnetic field for the many-body model. Thermal noise as expected would lead to broadening of the states and destroy the phase coherence required to maintain significant spin-spin interaction between the many-body states of the molecular moeity and that of the bulk electrode leading to attenuation of Kondo resonance [53, 57, 81]. Similarly magnetic field even though naively should split the ground state into two (Zeeman splitting), low field sublinear scaling of the energy width [53, 57, 82, 83] can be explained through the barrier to decimate the usual resonant Kondo interactions leading to a global many-body singlet state. Such effects if incorporated for future analysis into the many-body framework discussed here, at least for systems with significant orbital degeneracies as in the complex studied for which the single-level Anderson picture would be insufficient , would offer a new paradigm to discuss Kondo physics in tunnel-coupled junctions.

3.5 Energetics of conductance switching in pH sensors

To compete with silicon-based electronics, one of the most actively pursued avenue for scientific exploration is identification and development of robust conductance switching in nanoscopic conductors for using them in next-generation data storage and logical circuitry. Fortunately, diverse structural tunability in molecular systems have already us gifted several viable candidates for switching action which respond to a plethora of external physical stimulus like temperature[84], photon-induced transformations[85, 86],tunelling current[87] and mechanical forces[88]. Similarly conductance switching due to chemical modifications[89, 90] have also been studied with those susceptible to even the displacement of small atomistic units like single protons [91, 92]. Adding to the latter list is a recent experiment on 4,4-vinylbipyridine (4,4-VBP) in Ni contacts[93] wherein conductance switching due to pH sensitivity has been reported first ever. Motivated by this study, in this contribution we the-

oretically analyze the structurally isomorphic family of 4,4-bipyridine(4,4-BP) which can toggle reversibly between tristable states due to proton-exchange equilibrium(see Fig. 3.13) emphasizing the role of energetics in the process through many-body explanations hitherto unseen.

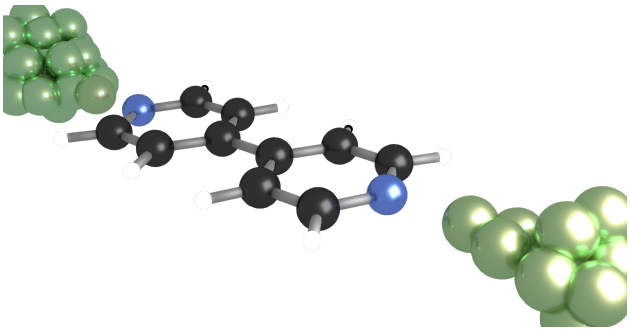

Figure 3.13: The 4,4,-bipyridine molecule (4,4-BP) studied in this report capped with Ni electrodes (green). The carbon atoms are in black, nitrogens in blue and the hydrogens in grey. The two conjugate acids(4,4-BPH^{+} and 4,4-BPH$_2^{+2}$) are obtained by protonating the two nitrogen centers successively.

The recently developed current constrained variational principle[71] in a correlated electronic structure framework quantifies the potential required to maintain an average flux in a molecular conductor as follows:

$$V = L\left(\frac{\Delta E_{\text{curr}}}{\alpha}\right)^{1/2} \tag{3.2}$$

where L is the length of the molecule and lead combination, α is the zero-field polarizability obtained by turning a spatially steady electric field and ΔE_{curr} is the response required to maintain the flux (see Methods for details) . In this report we therefore apply the method to unravel the role of these key parameters on dictating the conductance signatures in the neutral and the protonated forms of 4,4-bipyridine and explain the results through computation of the actual excited state manifold [72] which sheds important insight on the energetics of the event. The neutral base has been extensively studied before in single molecular junctions clipped with gold electrodes[88, 94–96] and recently even with nickel contacts[97]. The

molecular parameters for the neutral base (4,4-BP) and its corresponding monoprotonated (4,4-BPH^{+}) and diprotonated (4,4-BPH_2^{+2}) conjugate acids are obtained through ground state geometry optimization using DFT/B3LYP in 6-31G* basis set. The calculations also involve two Ni atomic centers placed 2.0$\mathring{A}$ apart from the axial N atoms of the bipyridine moeities as representations of the electrode similar to a recent study of pH sensitivity to conductance of 4,4-vinyl bipyridine (4,4-VBP)[93] using the said electrode set-up. The basis set used is LANL2Dz for Ni with effective core potential(ECP) and 6-311G for N, 6-31G for C and H. Since the charges on the studied systems are acquired through proton-shift equilibrium only, all species have the same even number of electrons and are all spin-singlet in their respective ground states. We use a subset of the N-representability constraints known as the 2-positivity conditions [3, 5, 6]. The neutral specie is treated using an active-space formulation [1] of the aforementioned semi-definite scheme in PySCF in a space of [16e, 16o]. Similar active space with maximum overlap with the neutral form was used for the protonated forms too. The active orbitals for both the systems involves energetically frontier states of π (having the p orbitals of the C and N atoms and the dxy of the metals) and σ symmetry (lone pair on N and the dz^2 on Ni for the neutral form. For the protonated ones it has contribution from H s orbitals too.) involving the metal centers and the atoms of the pyridine moeities. The excited state computations for each specie were done using an algorithm under development by one of the co-authors[72].To compute the zero-field polarizabilities for the ground states, CCSD calculations in GAMESS electronic structure package was used correlating all but the 30 inner core orbitals for all the three species.

In Ref[93], single-molecular conductances of 4,4-VBP and its conjugate acids were modulated using both pH as well as gate potential using a three-terminal device. It was seen that negative gate potential and lower pH favored the formation of the protonated forms which is justifiable from electrostatic considerations and basic principles of proton-shift equilibrium. The protonated forms (which was conjectured to be the monopositive conjugate acid only) was found to display remarkably less conductance compared to the neutral base. It was also

anticipated that a similar effect would be seen in the close-cousin i.e. 4,4-BP family at a lower pH owing to the lower pKa values of the molecules[98]beyond what was used in the said experiment .To investigate the claim, in Fig.3.14 we plot the I vs V curves for all the three species of the said family using our current-constrained variational principle. Consistent with expectations, we indeed see that the conjugate acids require higher potential to support the average flux compared to the neutral form.

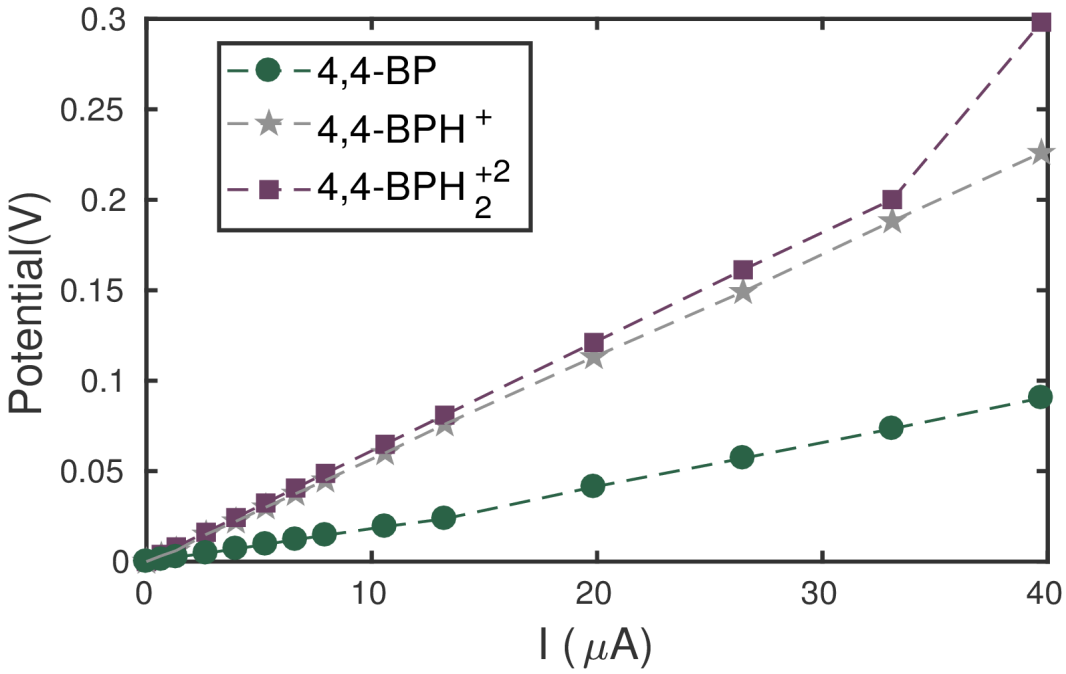

Figure 3.14: The I vs V plot of the neutral base (4,4-BP), the unipositive (4,4-BPH$^+$) and the dipositive (4,4-BPH$_2^{+2}$). While the neutral form requires much less potential to maintain the average flux due to the combined effect of low excited state gap and enhanced zero-field polarizability, among the conjugate acids the diprotonated form is slightly less conducting primarily due to the effect of zero-field polarizability and less transmission(see text)

Even though the zero-bias conductance from the I vs V plot in Fig.3.14 might seem to be high compared to previous reports of 4,4-VBP [93]or 4,4-BP in Au junctions[88, 94–96] or even in Ni junction[97], we capture the qualitative trend right. Justification for the high conductance with respect to 4,4-VBP can be attributed to several factors like slightly higher

length of 4,4-VBP compared to 4,4-BP and higher uncertainity associated with solution phase study of the recent experiment[93] unlike a single-molecular gas phase analysis of 4,4-BP presented here whereas the differences from Au coupled junctions in 4,4-BP are likely due to a high geometric diversity[88, 94–96]. Although it was reported in 4,4-BP in Ni junctions that the tilted geometrical form had similar conductance as the linear form[97] and a spin-polarized model of transport was used to explain the data from the experiment, whether both the assertions carry over to the protonated conjugate acids is unknown and is open to future experimental investigation. In absence of such atomistic details, we have used the optimized equilibrium ground state geometry (wherein the pyridine units are co-planar) for each of the three species without any spin-resolved study for a fair comparison.

Table 3.5: Comparison of the changes in Mulliken charges for the various moeities in 4,4-BPH(neutral base), 4,4-BPH^+ (monoprotonated acid) and 4,4-BPH_2^{+2} (diprotonated acid). Absolute Mulliken charges for 4,4-BP are presented whereas only the relative charges (Δ) with respect to the neutral base are displayed for the two protonated forms.

Groups/Atoms	Mulliken charge	Δ	
	4,4-BP	4,4-BPH^+	4,4-BPH_2^{+2}
Ni(1)	−0.12488	0.99655	0.26273
Ni(2)	−0.12488	0.17171	0.26273
$C_5H_4N(1)$	0.12488	-0.34126^a	0.73728^a
$C_5H_4N(2)$	0.12488	0.17302	0.73728^a

$^a C_5H_4NH^+$.

The trend is usually attributed to the depleting transmission of electronic density in the charged species relative to the neutral one which is evident even from Table 3.5 wherein the Ni contacts do gain significant positive charges in the conjugate acids. The pyridinium unit($C_5H_4NH^+(1)$) in the unipositive acid due to the enhanced electronegativity after protonation attracts a fair share of electron density towards itself thereby depleting the connecting Ni atom (Ni(1)) and even the pristine pyridine moeity ($C_5H_4N(2)$).The diprotonated form displays a far more equitable distribution of electron density due to regain of symmetry with both the pyridinium moieties and the two nickel atoms bleeding to account for the two pos-

itive charges. Indeed this justifies the fact that the fraction of average flux (ϕ) maintained on the Ni contacts in column 4 of Table 3.6 plummets with the increasing charge on the substrate as the supporting electron density depletes. In Ref[93] using the functional relationship of the surface concentration of the adsorbed protonated form and the neutral base against the local pH and gate voltage applied they were able to determine the fraction of the charge on the adsorbates (assuming Langmuir model). It was asserted that only a portion of the positive charge will be retained in the molecular backbone of the conjugate acid of 4,4-VBP (restricted to the monoprotonated form) with the remaining being dispersed to the Ni electrode set-up (see Fig.3 in Ref [93]). From Table 3.5, we also see the emergence of this claim too from a microscopic standpoint with the enhancing Mulliken charges on the Ni contacts post protonation.

However, apart from the said effect which do favor the neutral base in our analysis, to delve into the energetic details of the process, in column 3 of Table 3.6 we also display the re-organization cost (ΔE_{curr}) i.e. the change in many-body energy required to maintain the flux for each of the three species along with their zero-field electric polarizability (α). The low values for the re-organization energies (explicating the high conductance) indicates that only a significant mixing of the first excited state with the ground state is relevant for the cost incurred.

To analyze this energetic penalty in details, in Fig.3.15 we thus plot the *many body* DOS obtained from a recently developed algorithm by one of the co-authors [72] using the ground state guess from a variational 2RDM calculation. We see that the first excited state for the neutral form is much closer to the ground state compared to the charged forms thereby facilitating better mixing and explaining the low energetic cost. The zero-field polarizability (column 5 of Table 3.6) coupled with the enhanced transmission relative to the cationic acids only further augments the effect. However between the two conjugate acids, even though the energy gap between the ground and the first excited state is higher for the monoprotonated form than the diprotonated one (thereby explaining the slightly higher energetic cost of

Table 3.6: The energetic cost ($\triangle$ E_{curr}) for maintaining the flux along with zero field polarizability (α) and the fraction of the average current ($\phi = \frac{I_{tr}}{I_{avg}}$) maintained at the Ni contacts for the three species. Due to linearity in I_{tr} versus I_{avg}, the fraction is the same for all I_{avg}. It is clear that ϕ decreases with the increasing positive charge on the system (see Table 3.5). Also $\triangle$ E_{curr} for the neutral 4,4-BP is lesser than its conjugate acids due to low excited state energy gap (see Fig.3). Among the charged species, $\triangle$ E_{curr} for the unipositive one is slightly larger (see Fig.3 and text) but the zero-field polarizability (α) favors it dictating the trend.

System	I(μ A)	$\triangle$ E_{curr}	$\phi = \frac{I_{tr}}{I_{avg}}$	α
4,4-BP	6.62	9.042×10^{-8}	0.513	567.4
	13.24	3.434×10^{-7}		
	26.48	2.003×10^{-6}		
4,4-BPH^{+}	6.62	7.548×10^{-7}	0.116	495.2
	13.24	3.089×10^{-6}		
	26.48	1.191×10^{-5}		
4,4-BPH_2^{+2}	6.62	4.041×10^{-7}	0.075	225.8
	13.24	1.601×10^{-6}		
	26.48	6.351×10^{-6}		

the former than the latter), the competing effect of zero-field electronic polarizability of 4,4-BPH^{+} being higher than 4,4-BPH_2^{+2} (see column 5 of Table 3.6), favors the former marginally in accordance with Eq.(1). We speculate that this two competing effect is also prevalent in 4,4-VBP which is responsible for the lack of clear resolvability of the dication peak from the monocation [93].

In this contribution, we have thus analyzed the various factors responsible for controlling the conductance switching trend in the family of 4,4-BP and its conjugate acids. We saw that percentage of the transmitted current, zero-field polarizability and the energetic cost for the conduction event due to a low-lying excited state all favors the neutral base (4,4-BP) which is the 'on' state relative to the protonated forms ('off' states). Among the two conjugate acids, the difference is marginal due to competing factors. Such detailed breakdown of the energetics of the process which differentiate the 'on' and 'off' states are not known to the best of our knowledge and can not only advance our understanding about single-molecular conduction in general but also facilitate rational design of such molecular machines with

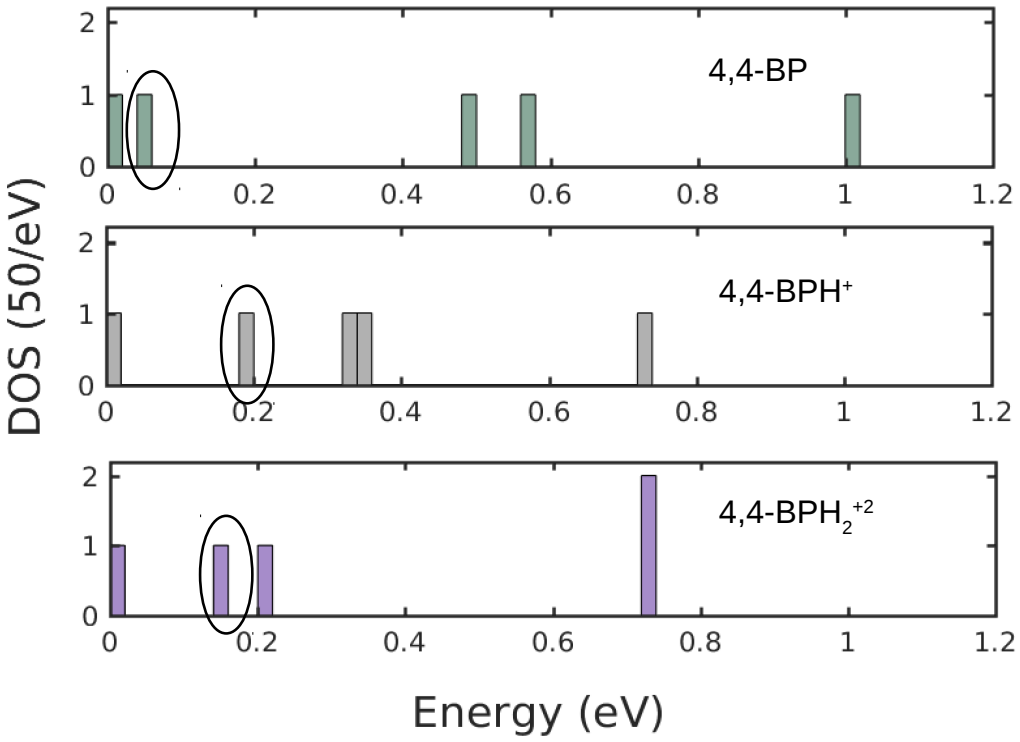

Figure 3.15: The DOS associated with the first few many-body excited states of all the three species studied. The unit indicates 50 states per eV of energy. It is clear from the low energy cost in Table 3.6 that its is the first excited state which is relevant for mixing with the ground state to maintain the imposed flux. We see that for the neutral form (4,4-BP) the said state (highlighted) is very close to the ground state which explains the low energetic cost (see column 3 of Table 3.6) and hence higher conductance('on' state). Among the conjugate acids, the diprotonated form (4,4-BPH_2^{+2}) has a slightly red-shifted excited state gap (with a close lying second excited state too) relative to the monoprotonated ion (4,4-BPH^+) explaining the slightly less energetic cost of the former in Table 3.6. Thus the conductance in this is dictated solely by the higher polarizability and less transmission (see Table I and S2).

robust switching functionality and in the development of future pH sensors which are of paramount importance as biological probes[99, 100].

3.6 References

[1] G. Gidofalvi and D. A. Mazziotti, J. Chem. Phys. **129**, 134108 (2008).

[2] A. J. Coleman, Rev. Mod. Phys. **35**, 668 (1963).

[3] D. A. Mazziotti, ed., *Reduced-Density-Matrix Mechanics: With Application to Many-Electron Atoms and Molecules (Advances in Chemical Physics)*, vol. 134 (Wiley: New York, 2007).

[4] D. A. Mazziotti, Phys. Rev. Lett. **108**, 263002 (2012), URL `https://link.aps.org/doi/10.1103/PhysRevLett.108.263002`.

[5] D. A. Mazziotti, Phys. Rev. Lett. **93**, 213001 (2004).

[6] D. A. Mazziotti, Phys. Rev. Lett. **106**, 083001 (2011).

[7] M. X. Goemans and D. P. Williamson, J. Comput. Syst. Sci. **68**, 442 (2004), ISSN 0022-0000.

[8] H. Angliker, E. Rommel, and J. Wirz, Chem. Phys.Lett **87**, 208 (1982).

[9] K. N. Houk, P. S. Lee, and M. Nendel, J. Org. Chem. **66**, 5517 (2001).

[10] L. Greenman and D. A. Mazziotti, J. Chem. Phys. **130**, 184101 (2009).

[11] K. Pelzer, L. Greenman, G. Gidofalvi, and D. A. Mazziotti, J. Phys. Chem. A. **115**, 5632 (2011), `http://dx.doi.org/10.1021/jp2017192`.

[12] W. J. Hehre, R. F. Stewart, and J. A. Pople, J. Chem. Phys. **51**, 2657 (1969).

[13] S. Moret and L. S. Conte, J. Chromatogr. A **882**, 245 (2000).

[14] A. Tielens, Annu. Rev. Astron. Astr. **46**, 289 (2008).

[15] T. C. Wu, N. J. Thompson, D. N. Congreve, E. Hontz, S. R. Yost, T. Van Voorhis, and M. A. Baldo, Appl. Phys. Lett **104**, (2014).

[16] P. M. Zimmerman, F. Bell, D. Casanova, and M. Head-Gordon, J. Am. Chem Soc. **133**, 19944 (2011).

[17] C. Dimitrakopoulos and P. Malenfant, Adv. Mater. **14**, 99 (2002).

[18] C. Reese, M. Roberts, M. mang Ling, and Z. Bao, Mater. Today **7**, 20 (2004).

[19] R. Yamada, H. Kumazawa, T. Noutoshi, S. Tanaka, and H. Tada, Nano Letters **8**, 1237 (2008), pMID: 18311936, https://doi.org/10.1021/nl0732023, URL https://doi.org/10.1021/nl0732023.

[20] S. Ho Choi, B. Kim, and C. D. Frisbie, Science **320**, 1482 (2008), ISSN 0036-8075, http://science.sciencemag.org/content/320/5882/1482.full.pdf, URL http://science.sciencemag.org/content/320/5882/1482.

[21] B. Kim, S. H. Choi, X.-Y. Zhu, and C. D. Frisbie, Journal of the American Chemical Society **133**, 19864 (2011).

[22] T. Tada, D. Nozaki, M. Kondo, S. Hamayama, , and K. Yoshizawa*, J. Am. Chem. Soc. **126**, 14182 (2004).

[23] . Revital Cohen, . Kurt Stokbro, . Jan M. L. Martin, , and . Mark A. Ratner*, J.Phys.Chem. C **111**, 14893 (2007), http://dx.doi.org/10.1021/jp0795309.

[24] M. Magoga and C. Joachim, Phys. Rev. B **56**, 4722 (1997), URL http://link.aps.org/doi/10.1103/PhysRevB.56.4722.

[25] J. R. Quinn, J. Frank W. Foss, L. Venkataraman, M. S. Hybertsen, and R. Breslow, Journal of the American Chemical Society **129**, 6714 (2007).

[26] T. Yelin, R. Korytar, N. Sukenik, R. Vardimon, B. Kumar, C. Nuckolls, F. Evers, and O. Tal, Nat Mater **15**, 444 (2016).

[27] X. Xiao, B. Xu, and N. J. Tao, Nano Lett. **4**, 267 (2004).

[28] J. Ulrich, D. Esrail, W. Pontius, L. Venkataraman, D. Millar, and L. H. Doerrer, J. Phys. Chem. B **110**, 2462 (2006).

[29] M. Tsutsui, M. Taniguchi, and T. Kawai, Nano Lett. **9**, 2433 (2009).

[30] M. Tsutsui, Y. Teramae, S. Kurokawa, and A. Sakai, Appl. Phys. Lett. **89**, 163111 (2006).

[31] C. Bruot, J. Hihath, and N. J. Tao, Nat. Nanotechnol pp. 35–40 (2012).

[32] A. M. Bratkovsky and P. E. Kornilovitch, Phys. Rev. B **67**, 115307 (2003), URL `https://link.aps.org/doi/10.1103/PhysRevB.67.115307`.

[33] P. Delaney and J. C. Greer, Phys. Rev. Lett. **93**, 036805 (2004), URL `https://link.aps.org/doi/10.1103/PhysRevLett.93.036805`.

[34] H. Kondo, H. Kino, J. Nara, T. Ozaki, and T. Ohno, Phys. Rev. B **73**, 235323 (2006).

[35] E. P. Hoy, D. A. Mazziotti, and T. Seideman, J. Chem. Phys. **147**, 184110 (2017).

[36] M. Di Ventra, S. T. Pantelides, and N. D. Lang, Phys. Rev. Lett. **84**, 979 (2000), URL `https://link.aps.org/doi/10.1103/PhysRevLett.84.979`.

[37] K. Varga, Phys. Rev. B **83**, 195130 (2011).

[38] K. Stokbro, J. Taylor, M. Brandbyge, J.-L. Mozos, and P. Ordejn, Comput. Mater. Sci. **27**, 151 (2003).

[39] M. Smeu, R. A. Wolkow, and G. A. DiLabio, J. Chem. Phys. **129**, 034707 (2008).

[40] D. A. Mazziotti, Phys. Rev. Lett. **117**, 153001 (2016), URL https://link.aps.org/doi/10.1103/PhysRevLett.117.153001.

[41] M. A. Reed, C. Zhou, C. J. Muller, T. P. Burgin, and J. M. Tour, Science **278**, 252 (1997), ISSN 0036-8075.

[42] L. Venkataraman, J. E. Klare, I. W. Tam, C. Nuckolls, M. S. Hybertsen, and M. L. Steigerwald, Nano Lett. **6**, 458 (2006).

[43] F. Evers, F. Weigend, and M. Koentopp, Phys. Rev. B **69**, 235411 (2004), URL https://link.aps.org/doi/10.1103/PhysRevB.69.235411.

[44] S. Y. Quek, L. Venkataraman, H. J. Choi, G. Steven., M. S. Hybertsen, and J. B. Neaton, Nano Lett. **7**, 3477 (2007).

[45] A. Yamada, Q. Feng, A. Hoskins, K. D. Fenk, and B. D. Dunietz, Nano. Lett. **16**, 6092 (2016).

[46] K. Horiguchi, T. Sagisaka, S. Kurokawa, and A. Sakai, J. Appl. Phys. **113**, 144313 (2013).

[47] L. Venkataraman, Y. S. Park, A. C. Whalley, C. Nuckolls, M. S. Hybertsen, and M. L. Steigerwald, Nano Letters **7**, 502 (2007), pMID: 17253760, https://doi.org/10.1021/nl062923j, URL https://doi.org/10.1021/nl062923j.

[48] W. de Haas, J. de Boer, and G. van dn Berg, Physica **1**, 1115 (1934), ISSN 0031-8914, URL http://www.sciencedirect.com/science/article/pii/S0031891434803102.

[49] J. Kondo, Progress of Theoretical Physics **32**, 37 (1964), URL http://dx.doi.org/10.1143/PTP.32.37.

[50] J. Appelbaum, Phys. Rev. Lett. **17**, 91 (1966), URL https://link.aps.org/doi/10.1103/PhysRevLett.17.91.

[51] T. K. Ng and P. A. Lee, Phys. Rev. Lett. **61**, 1768 (1988), URL https://link.aps.org/doi/10.1103/PhysRevLett.61.1768.

[52] P. Nordlander, M. Pustilnik, Y. Meir, N. S. Wingreen, and D. C. Langreth, Phys. Rev. Lett. **83**, 808 (1999), URL https://link.aps.org/doi/10.1103/PhysRevLett.83.808.

[53] D. Goldhaber-Gordon, H. Shtrikman, D. Mahalu, D. Abusch-Magder, U. Meirav, and M. A. Kastner, Nature **391**, 156 (1998), URL http://dx.doi.org/10.1038/34373.

[54] J. Li, W.-D. Schneider, R. Berndt, and B. Delley, Phys. Rev. Lett. **80**, 2893 (1998), URL https://link.aps.org/doi/10.1103/PhysRevLett.80.2893.

[55] V. Madhavan, W. Chen, T. Jamneala, M. F. Crommie, and N. S. Wingreen, Science **280**, 567 (1998), ISSN 0036-8075, URL http://science.sciencemag.org/content/280/5363/567.

[56] J. Park, A. N. Pasupathy, J. I. Goldsmith, C. Chang, Y. Yaish, J. R. Petta, M. Rinkoski, J. P. Sethna, H. D. Abrua, P. L. McEuen, et al., Nature **417**, 722 (2002), URL http://dx.doi.org/10.1038/nature00791.

[57] W. Liang, M. P. Shores, M. Bockrath, J. R. Long, and H. Park, Nature **417**, 725 (2002), URL http://dx.doi.org/10.1038/nature00790.

[58] A. Zhao, Q. Li, L. Chen, H. Xiang, W. Wang, S. Pan, B. Wang, X. Xiao, J. Yang, J. G. Hou, et al., Science **309**, 1542 (2005), ISSN 0036-8075, URL http://science.sciencemag.org/content/309/5740/1542.

[59] Y.-S. Fu, S.-H. Ji, X. Chen, X.-C. Ma, R. Wu, C.-C. Wang, W.-H. Duan, X.-H. Qiu, B. Sun, P. Zhang, et al., Phys. Rev. Lett. **99**, 256601 (2007), URL https://link.aps.org/doi/10.1103/PhysRevLett.99.256601.

[60] Y.-h. Zhang, S. Kahle, T. Herden, C. Stroh, M. Mayor, U. Schlickum, M. Ternes, P. Wahl, and K. Kern, Nature Communications **4**, 2110 (2013), URL http://dx.doi.org/10.1038/ncomms3110.

[61] S. Sasaki, S. Amaha, N. Asakawa, M. Eto, and S. Tarucha, Phys. Rev. Lett. **93**, 017205 (2004), URL https://link.aps.org/doi/10.1103/PhysRevLett.93.017205.

[62] P. Jarillo-Herrero, J. Kong, H. S. van der Zant, C. Dekker, L. P. Kouwenhoven, and S. De Franceschi, Nature **434**, 484 (2005), URL http://dx.doi.org/10.1038/nature03422.

[63] M. Karolak, D. Jacob, and A. I. Lichtenstein, Phys. Rev. Lett. **107**, 146604 (2011), URL https://link.aps.org/doi/10.1103/PhysRevLett.107.146604.

[64] A. J. Keller, S. Amasha, I. Weymann, C. P. Moca, I. G. Rau, J. A. Katine, H. Shtrikman, G. Zarnd, and D. Goldhaber-Gordon, Nature Physics **10**, 145 (2013), URL http://dx.doi.org/10.1038/nphys2844.

[65] Y. Okazaki, S. Sasaki, and K. Muraki, Phys. Rev. B **84**, 161305 (2011), URL https://link.aps.org/doi/10.1103/PhysRevB.84.161305.

[66] E. Minamitani, N. Tsukahara, D. Matsunaka, Y. Kim, N. Takagi, and M. Kawai, Phys. Rev. Lett. **109**, 086602 (2012), URL https://link.aps.org/doi/10.1103/PhysRevLett.109.086602.

[67] R.-N. Shang, T. Zhang, G. Cao, H.-O. Li, M. Xiao, G.-C. Guo, and G.-P. Guo, Phys. Rev. B **97**, 085307 (2018), URL https://link.aps.org/doi/10.1103/PhysRevB.97.085307.

[68] D. Krychowski and S. Lipiński, Phys. Rev. B **93**, 075416 (2016), URL https://link.aps.org/doi/10.1103/PhysRevB.93.075416.

[69] S. Bock, A. Liluashvili, and T. Gasenzer, Phys. Rev. B **94**, 045108 (2016), URL https://link.aps.org/doi/10.1103/PhysRevB.94.045108.

[70] M. Lee, M.-S. Choi, R. López, R. Aguado, J. Martinek, and R. Žitko, Phys. Rev. B **81**, 121311 (2010), URL https://link.aps.org/doi/10.1103/PhysRevB.81.121311.

[71] M. Sajjan and D. A. Mazziotti, Communications Chemistry **1**, 31 (2018), URL https://doi.org/10.1038/s42004-018-0030-2.

[72] S. Hemmatiyan, M. Sajjan, A. Schlimgen, and A. Mazziotti, David, J. Phys. Chem. Lett. (Submitted) (2018).

[73] G. Stefanucci and S. Kurth, Phys. Rev. Lett. **107**, 216401 (2011), URL https://link.aps.org/doi/10.1103/PhysRevLett.107.216401.

[74] A. W. Schlimgen, C. W. Heaps, and D. A. Mazziotti, J. Phys. Chem. Lett. **7**, 627 (2016).

[75] J. M. Montgomery and D. A. Mazziotti, The Journal of Physical Chemistry A **122**, 4988 (2018), pMID: 29771514, https://doi.org/10.1021/acs.jpca.8b00941, URL https://doi.org/10.1021/acs.jpca.8b00941.

[76] L. Greenman and D. A. Mazziotti, J. Chem. Phys. **133**, 164110 (2010).

[77] M. P. Shores and J. R. Long, Journal of the American Chemical Society **124**, 3512 (2002), pMID: 11929233, https://doi.org/10.1021/ja025512n, URL https://doi.org/10.1021/ja025512n.

[78] J. Bonča and J. E. Gubernatis, Phys. Rev. B **47**, 13137 (1993), URL https://link.aps.org/doi/10.1103/PhysRevB.47.13137.

[79] A. W. Schlimgen and D. A. Mazziotti, J. Phys. Chem. A **121**, 9377 (2017).

[80] G. D. Scott and D. Natelson, ACS Nano **4**, 3560 (2010), pMID: 20568709, https://doi.org/10.1021/nn100793s, URL https://doi.org/10.1021/nn100793s.

[81] L. H. Tjeng, S.-J. Oh, E.-J. Cho, H.-J. Lin, C. T. Chen, G.-H. Gweon, J.-H. Park, J. W. Allen, T. Suzuki, M. S. Makivić, et al., Phys. Rev. Lett. **71**, 1419 (1993), URL https://link.aps.org/doi/10.1103/PhysRevLett.71.1419.

[82] T. A. Costi, Phys. Rev. Lett. **85**, 1504 (2000), URL https://link.aps.org/doi/10.1103/PhysRevLett.85.1504.

[83] M. Filippone, C. u. u. u. u. P. m. c. Moca, J. von Delft, and C. Mora, Phys. Rev. B **95**, 165404 (2017), URL https://link.aps.org/doi/10.1103/PhysRevB.95.165404.

[84] S. Weigelt, C. Busse, L. Petersen, E. Rauls, B. Hammer, K. V. Gothelf, F. Besenbacher, and T. R. Linderoth, Nature Materials **5**, 112 (2006).

[85] M. J. Comstock, N. Levy, A. Kirakosian, J. Cho, F. Lauterwasser, J. H. Harvey, D. A. Strubbe, J. M. J. Fréchet, D. Trauner, S. G. Louie, et al., Phys. Rev. Lett. **99**, 038301 (2007), URL https://link.aps.org/doi/10.1103/PhysRevLett.99.038301.

[86] C. Jia, A. Migliore, N. Xin, S. Huang, J. Wang, Q. Yang, S. Wang, H. Chen, D. Wang, B. Feng, et al., Science **352**, 1443 (2016), ISSN 0036-8075, URL http://science.sciencemag.org/content/352/6292/1443.

[87] V. Iancu and S.-W. Hla, Proceedings of the National Academy of Sciences **103**, 13718 (2006), ISSN 0027-8424, http://www.pnas.org/content/103/37/13718.full.pdf, URL http://www.pnas.org/content/103/37/13718.

[88] S. Y. Quek, M. Kamenetska, M. L. Steigerwald, H. J. Choi, S. G. Louie, M. S. Hybertsen, J. B. Neaton, and L. Venkataraman, Nature Nanotechnology **4**, 230 (2009), URL http://dx.doi.org/10.1038/nnano.2009.10.

[89] T. A. Su, H. Li, M. L. Steigerwald, L. Venkataraman, and C. Nuckolls, Nature Chemistry **7**, 215 (2015), URL http://dx.doi.org/10.1038/nchem.2180.

[90] X. Yin, Y. Zang, L. Zhu, J. Z. Low, Z.-F. Liu, J. Cui, J. B. Neaton, L. Venkataraman, and L. M. Campos, Science Advances **3** (2017), URL http://advances.sciencemag.org/content/3/10/eaao2615.

[91] G. J. Simpson, S. W. L. Hogan, M. Caffio, C. J. Adams, H. Frchtl, T. van Mourik, and R. Schaub, Nano Letters **14**, 634 (2014), pMID: 24471795, https://doi.org/10.1021/nl4038517, URL https://doi.org/10.1021/nl4038517.

[92] W. Auwrter, K. Seufert, F. Bischoff, D. Ecija, S. Vijayaraghavan, S. Joshi, F. Klappenberger, N. Samudrala, and J. V. Barth, Nature Nanotechnology **7**, 41 (2011), URL http://dx.doi.org/10.1038/nnano.2011.211.

[93] R. J. Brooke, D. S. Szumski, A. Vezzoli, S. J. Higgins, R. J. Nichols, and W. Schwarzacher, Nano Letters **18**, 1317 (2018), https://doi.org/10.1021/acs.nanolett.7b04995, URL https://doi.org/10.1021/acs.nanolett.7b04995.

[94] . J. Prez-Jimnez, The Journal of Physical Chemistry B **109**, 10052 (2005), pMID: 16852216, https://doi.org/10.1021/jp044370b, URL https://doi.org/10.1021/jp044370b.

[95] Z. Liu, S.-Y. Ding, Z.-B. Chen, X. Wang, J.-H. Tian, J. R. Anema, X.-S. Zhou, D.-Y. Wu, B.-W. Mao, X. Xu, et al., Nature Communications **2**, 305 (2011), URL http://dx.doi.org/10.1038/ncomms1310.

[96] T. Kim, P. Darancet, J. R. Widawsky, M. Kotiuga, S. Y. Quek, J. B. Neaton, and L. Venkataraman, Nano Letters

14, 794 (2014), https://doi.org/10.1021/nl404143v, URL https://doi.org/10.1021/nl404143v.

[97] R. J. Brooke, C. Jin, D. S. Szumski, R. J. Nichols, B.-W. Mao, K. S. Thygesen, and W. Schwarzacher, Nano Letters **15**, 275 (2015), https://doi.org/10.1021/nl503518q, URL https://doi.org/10.1021/nl503518q.

[98] T. R. Musgrave and C. E. Mattson, Inorganic Chemistry **7**, 1433 (1968), https://doi.org/10.1021/ic50065a035, URL https://doi.org/10.1021/ic50065a035.

[99] S. Surana, J. M. Bhat, S. P. Koushika, and Y. Krishnan, Nature Communications **2**, 340 (2011), URL http://dx.doi.org/10.1038/ncomms1340.

[100] P. Shrestha, Y. Cui, J. Wei, S. Jonchhe, and H. Mao, Analytical Chemistry **90**, 1718 (2018), https://doi.org/10.1021/acs.analchem.7b03478, URL https://doi.org/10.1021/acs.analchem.7b03478.

CHAPTER 4

ENTANGLING AND DISENTANGLING MANY-ELECTRON QUANTUM SYSTEMS WITH A SPATIALLY HOMOGENEOUS ELECTRIC FIELD

This chapter contains parts of an article that was originally published in the Physical Review A. Reproduced with permission from [M.Sajjan, K. H. Marsden, and D. A. Mazziotti, *Phys.Rev.A*, **97**, 062502 (2018)].

4.1 Introduction

The expectation values of many-body product operators for two or more subsystems of a pure-state quantum system can become inseparable in a process known as *entanglement*. Formally, entanglement is present between two subsystems in the pure-state of a many-electronic quantum system when the system's density matrix cannot be expressed as an anti-symmetrized product of the subsystems' density matrices [1–3] which is equivalent to the inability to express the many-body state using a single Slater determinantal ansatz. This in turn fosters *correlation* in electronic properties. In addition to the computation of electron correlation, a significant challenge in quantum theory is the control of a molecule's electron correlation [4–7]. In this chapter we show that the degree of electron correlation and entanglement in quantum molecular systems can be controlled through an external stimulus such as an electric field.

The application of an electric field in the direction parallel to a molecule's dipole moment, we show computationally, decreases the degree of electron correlation in the molecule, and conversely, the application of an electric field in the direction opposite to a molecule's dipole moment increases the degree of electron correlation in the molecule. More generally, using the set of one-electron reduced density matrices (1-RDMs) and notions of convexity, we prove mathematically that any external stimulus that significantly changes the expectation

value of a one-electron operator with non-degenerate minimum and maximum eigenvalues can be used to control the degree of electron correlation in the molecule. The concept is illustrated through calculations with the molecules HeH^+, MgH^+, BH, HCN, H_2O, HF, CH_2O, and a fluorescent dye. Furthermore, we show in calculations with formaldehyde (CH_2O) that the field can control not only the electron correlation of a formaldehyde molecule but also the entanglement among formaldehyde molecules in an array. The control of a molecule's correlation and entanglement has potential applications to designing molecules and materials with controllable properties as well as modifying the degree of correlation between fundamental units such as qubits in quantum computation.

4.2 Theory

The 1-RDM of a pure N-electron state is computable from the state's N-electron wavefunction

$$^1D(1,\bar{1}) = N \int \psi(123..N)\psi^*(\bar{1}23..N)d(23..N). \tag{4.1}$$

Such a 1-RDM is said to be *pure N-representable* [8–11]. Although the set of pure N-representable 1-RDMs is not convex, it is contained within the convex set of ensemble N-representable 1-RDMs [9]. A 1-RDM is *ensemble N-representable* if and only if it can be obtained from the integration of at least one ensemble N-electron density matrix [8, 12, 13]. Because the set is convex, all 1-RDMs within the set can be expressed as convex combinations of its extreme 1-RDMs [14]. Coleman proved the key result that the extreme 1-RDMs are the pure-state 1-RDMs whose wavefunctions are Slater determinants [8, 13]. Formally, the convex set of ensemble N-representable 1-RDMs is the *convex hull* of its extreme elements, $P_N^1 = \mathrm{Conv}(S_{\mathrm{Slater}})$ where S_{Slater} is the set of 1-RDMs whose N-electron pre-images are Slater determinants.

4.2.1 Revisiting Electronic Correlation

An N-electron quantum system is *correlated* if and only if its N-electron density matrix cannot be written as a product of the 1-RDMs in their natural-orbital basis set. This definition of electron correlation in the terminology of entanglement is equivalent to the conventional definition in which the wavefunction is inexpressible as a single Slater determinant. While entanglement is often associated with particles that are located at a great distance from each other, such large separation is not necessary for entanglement and not applicable in the case of electrons bound to a molecule [15]. In the next section we show that the *cumulant* of the 2-RDM is non-vanishing if and only if the N-electron density matrix is correlated. Furthermore, the von Neumann entropy of the 1-RDM is nonzero if and only if the cumulant of the 2-RDM does not vanish. Therefore, the von Neumann entropy of the 1-RDM is nonzero if and only if the quantum system exhibits electron correlation (entanglement of the N-electron density matrix with respect to the product of the 1-RDMs).

4.2.2 Quantification of Electronic Correlation

The cumulant (or connected) part ${}^2\Delta$ of the two-electron reduced density matrix (2-RDM) [3, 16–18] is defined as

$$ {}^2\Delta^{ij}_{kl} =^2 D^{ij}_{kl} - 2\,{}^1D^i_k \wedge {}^1D^j_l \tag{4.2} $$

in which ${}^1D$ and ${}^2D$ are the 1- and 2-RDMs, normalized to N and $N(N-1)$, and $\wedge$ is the antisymmetric tensor product known as the Grassmann wedge product [3, 19]. From the cumulant's definition in Eq. (4.2) we show below that its trace of can act as a measure of correlation [20–22]

Theorem: The trace of the cumulant part ${}^2\Delta$ of the 2-RDM is non-zero iff its a Hartree-Fock state i.e. a single Slater determinant resolved in the natural orbital basis (eigenbasis of the 1RDM)

Proof

$$\begin{aligned}
\mathrm{Tr}({}^2\Delta) &= \mathrm{Tr}({}^2D) - \mathrm{Tr}({}^1D \wedge {}^1D) \\
&= N(N-1) + \mathrm{Tr}({}^1D^2) - (\mathrm{Tr}({}^1D))^2 \qquad \because \mathrm{Tr}({}^2D) = N(N-1) \\
&= N(N-1) - N^2 + \mathrm{Tr}({}^1D^2) \qquad \because \mathrm{Tr}({}^1D) = N \\
&= \mathrm{Tr}({}^1D^2) - N \\
&= \mathrm{Tr}({}^1D({}^1I - {}^1Q)) - N \\
&= \mathrm{Tr}({}^1D) - \mathrm{Tr}({}^1D{}^1Q) - N \\
&= -\mathrm{Tr}({}^1D{}^1Q)
\end{aligned} \tag{4.3}$$

Thus for a Hartree-Fock state in the eigenbasis of the 1-RDM as ${}^1D^2 = {}^1D$ or ${}^1D{}^1Q = 0$, thus the $\mathrm{Tr}({}^2\Delta) = 0$. Now for the converse lets start with $\mathrm{Tr}({}^2\Delta) = 0$ as follows and see if it implies the Hartree-Fock state

$$\begin{aligned}
\mathrm{Tr}({}^2\Delta) &= 0 \\
-\mathrm{Tr}({}^1D{}^1Q) &= 0 \\
\mathrm{Tr}(A^\dagger AB^\dagger B) &= 0 \qquad \because {}^1D = A^\dagger A \succeq 0, {}^1Q = B^\dagger B \succeq 0 \\
\mathrm{Tr}((AB^\dagger)^\dagger AB^\dagger) &= 0 \\
||(AB^\dagger)||_F &= 0 \\
AB^\dagger &= \mathbf{0} \\
{}^1D{}^1Q &= A^\dagger AB^\dagger B = \mathbf{0} \\
{}^1D^2 = {}^1D &\implies \text{HFstate}
\end{aligned} \tag{4.4}$$

with ${}^1Q(= {}^1I - {}^1D)$ being the 1-hole RDM in terms of the 1-RDM and the identity

matrix ${}^1I$ and $\mathbf{0}$ is the null matrix. Thus the trace of ${}^1Q$ and ${}^1D$ vanishes only if they lie in orthogonal subspaces which is equivalent to the N eigenvectors of the 1-RDM (natural orbitals) being completely filled and the remaining eigenvectors (natural orbitals) being completely empty or the 1-RDM being representable by an N-electron Slater determinant and converse is also true. Consequently, we have that the trace of the cumulant 2-RDM vanishes if and only if the N-electron quantum system is not correlated [20]. Furthermore, because the magnitude of the trace of the cumulant 2-RDM reflects the degree to which natural orbitals are shared by both particles and holes, it provides a mechanism to quantify the degree of electron correlation.

The trace of the cumulant can be related to the von Neumann entropy [23–26] in Eq. (4.10) The natural logarithm of the 1-RDM can be expanded in a power series about the identity matrix

$$\begin{aligned} \ln({}^1D) &= \ln({}^1I - {}^1Q) && (4.5)\\ &= -\sum_{n=1}^{\infty} ({}^1Q)^n/n && (4.6)\\ &\approx -{}^1Q - \mathcal{O}({}^1Q^2). && (4.7) \end{aligned}$$

Substituting Eq. (4.7) into the von Neumann entropy in Eq. (4.10) and using Eq. (**??**) yields

$$S_1 = -\mathrm{Tr}({}^1\mathrm{D}\ln({}^1\mathrm{D})) \approx -\mathrm{Tr}({}^2\Delta) + \mathcal{O}(\mathrm{Tr}({}^1D({}^1Q)^2)) \geq 0. \quad (4.8)$$

Hence, we observe that the von Neumann entropy is equal to the negative of the trace of the cumulant 2-RDM through the terms scaling linearly with the 1-hole RDM. Like the negative of the trace of the cumulant 2-RDM, the von Neumann entropy is a nonnegative quantity which vanishes only in the absence of electron correlation (not only the first term but all successive terms as they are ${}^1D^n({}^1Q)^m$ with $n, m \in \mathcal{Z}_+$). The von Neumann entropy of the 1-RDM has been employed extensively in the literature [22, 27–36] as a measure of electron

correlation.

4.2.3 Controlling Electronic Correlation

In this section we show that any adjustable external stimulus that changes the expectation value of a one-electron operator ${}^1\hat{O}$ with non-degenerate minimum and maximum eigenvalues can be employed to control a molecule's electron correlation. To demonstrate this result, we will rely upon some key ideas from convexity and reduced-density-matrix theory.[12–14]. The expectation value of the one-electron operator ${}^1\hat{O}$ is expressible in terms of the 1-RDM:

$$\langle {}^1\hat{O} \rangle(\epsilon) = \mathrm{Tr}({}^1\hat{O}\ {}^1D(\epsilon)) \tag{4.9}$$

where ϵ is a controllable parameter such as an electric field for controlling the expectation value of $\hat{O}$. The ϵ controls the expectation value of $\hat{O}$ by changing ${}^1D(\epsilon)$ which is the 1-RDM of the ground state of the system with the stimulus ϵ. By convexity the minimum and maximum expectation values occur at one or more extreme 1-RDMs. Importantly, from Coleman's theorem [8] we know that these 1-RDMs are contained in S_{Slater}, the set of uncorrelated 1-RDMs. From these two observations we obtain the following theorem:

Theorem: If the operator ${}^1\hat{O}$ has a non-degenerate ground state, then there is a unique extreme 1-RDM in the uncorrelated set S_{Slater} for which the minimum expectation value of ${}^1\hat{O}$ is achieved.

Proof: Because the expectation value of a one-electron observable is an affine function of the 1-RDM, minimization of the expectation value over the convex set of 1-RDMs P_N^1 must occur at one or more extreme points. Because the operator ${}^1\hat{O}$ is assumed to have a non-degenerate ground state, the minimum must occur at a unique point. By Coleman's theorem the unique extreme point at which the minimum occurs must be a 1-RDM with a Slater-determinant pre-image, that is a 1-RDM in the uncorrelated set S_{Slater}.

Similarly, If the operator ${}^1\hat{O}$ has a non-degenerate maximal state, then there is a unique

extreme 1-RDM in the uncorrelated set S_{Slater} for which the maximum expectation value of ${}^1\hat{O}$ is achieved. Consequently, the expectation value of the operator ${}^1\hat{O}$ can be controlled with ϵ to steer the 1-RDM towards the uncorrelated extreme 1-RDM at which the expectation value reaches its minimum or maximum value.

Controllable 1-electron observables that correspond to non-degenerate 1-electron operators thus provide a general mechanism for modulating the electron correlation of a molecular system. In this chapter we use a static electric field as a continuous parameter for controlling the strength of the dipole moment,an 1-body observable, and hence the degree of the molecule's electron correlation. As the electric dipole moment is moved towards an extreme by the electric field, the 1-RDM moves toward the extreme 1-RDM corresponding to the Slater determinant with the minimum or maximum observable. Typically, a molecule with a greater polarizability will be more sensitive to the electric field, and hence, will exhibit greater changes in its electron correlation. Practically, the magnitude of the stimulus must be less than the value required to change the electronic identity of the molecule; in the case of the electric-field stimulus the field must be less than the value required to ionize the molecule. Figure 1 shows a schematic representation of the convex set of 1-RDMs. The color scheme of the set is chosen to represent its convexity with the most blue color (minimum value) and its yellow color (maximum value) occurring at the extreme points (extreme 1-RDMs) of the set. Changing the electric field steers the 1-RDM, represented by the dot, towards increasing or decreasing the dipole moment. In the direction towards the boundary of the set of 1-RDMs, the electric field decreases the electron correlation while in the opposite direction, the electric field increases the electron correlation.

4.3 Applications

After a discussion of computational methodology, we explore computationally the entangling and disentangling of molecules with an electric field through computations with two-electron systems HeH^+ and MgH^+ where only the two valence electrons of MgH^+ are correlated,

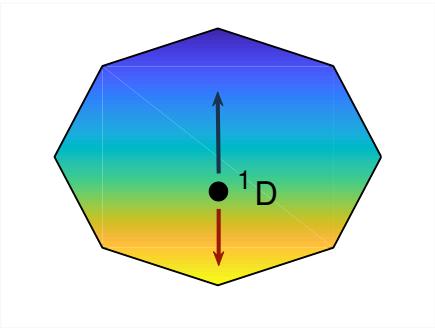

Figure 4.1: A schematic representation of the convex set of 1-RDMs is depicted. The color scheme of the set is chosen to represent its convexity with the most blue color (minimum value) and its most yellow color (maximum value) occurring at the extreme points (extreme 1-RDMs) of the set. Changing the electric field steers the 1-RDM, represented by the dot, towards increasing or decreasing the dipole moment. In the direction towards the boundary of the set of 1-RDMs, the electric field decreases the electron correlation while in the opposite direction, the electric field increases the electron correlation.

molecules BH, HCN, H_2O, and HF, the formaldehyde molecule CH_2O and an array of 6 formaldehyde molecules CH_2O, as well as a fluorescent dye mimic of VF2.1.H.

4.3.1 Computational Methodology

Molecular electronic structure calculations were performed on HeH^+, MgH^+, BH, HCN, H_2O, HF, formaldehyde, formaldehyde clusters, and a fluorescent dye. The two-electron calculation of HeH^+ was performed with full configuration interaction (FCI), and the calculation of MgH^+ was performed with a complete active-space configuration interaction (CASCI) using an active space of 2 electrons in 31 orbitals. For the larger molecules we employed the parametric two-electron reduced density matrix (2-RDM) method in which a parametrization of the 2-RDM is directly computed without the many-electron wavefunction [37–44]. The augmented correlation-consistent polarized valence double-zeta (aug-cc-pVDZ) basis set was employed for calculations of HeH^+, MgH^+, BH, HCN, H_2O, and HF the correlation-consistent polarized valence double-zeta (cc-pVDZ) basis set was employed for calculations of formaldehyde and the formaldehyde-cluster [45, 46], and the Dunning-Hay double-zeta

basis set was employed for the dye mimic [47]. The degree of electron correlation in the 1-RDM is quantified through its the von Neumann entropy [23], equivalent to its first-order Rényi entropy [24],

$$S_1 = -\mathrm{Tr}({}^1D \ln ({}^1D)) \tag{4.10}$$

or its second-order Rényi entropy [24, 48, 49].

$$S_2 = -\ln\left(\mathrm{Tr}({}^1D^2)\right). \tag{4.11}$$

As in Eq. (4.1), the 1-RDM is normalized to N. With this normalization the von Neumann entropy of the 1-RDM is a nonnegative quantity than vanishes only in the absence of electron correlation. While the 1-RDM can also be normalized to 1 in the definition of entropy, such a normalization produces an entropy that is not zero in the absence of electron correlation and that is not size consistent upon the doubling of the quantum system. Note that electron correlation, a form of entanglement, is not the same as the electron correlation energy, and that the relationship between these two quantities is nontrivial [2, 31, 32]. The second-order entropy provides experimentally accessible information [50]. In section 4.3.2 the notation ΔS_α will be used to indicate the difference in the entropy in the presence and the absence of an electric field ϵ, $\Delta S_\alpha = S_\alpha(\epsilon) - S_\alpha(0)$. The α-order Rényi entropy of cluster formation is given by

$$S_{\alpha,\mathrm{f}} = S_{\alpha,\mathrm{cluster}} - \sum_i S_{\alpha,i}, \tag{4.12}$$

where the summation is over the entropy of each of the individual molecules. The summation is permissible due to the additivity of the Rényi entropy for non-interacting constituents. The entropy of formation quantifies the excess quantum correlation that exists in the cluster due to the intermolecular bonding.

4.3.2 Results

We start the section by showing Full-CI results for BH in (aug-cc-pVDZ) basis. In Fig.4.2 we plot the change in Frobenius norm ($||^1\Delta||_F$) which is defined as the difference in the $||^1D - ^1D_{HF}||_F$ (actually the difference in the norm is computed with respect to its value at zero electric field strength hence $\Delta||^1\Delta||_F$) as a function of the angle (the angle is measured with respect to internuclear axis in BH with $\theta = 0$ corresponding to the direction of the dipole moment) for two specific values of field strength. We see the norm changes in an oscillatory (due to $C_{\infty v}$ symmetry of the system). For directions along the dipole the system gets decorrelated (the difference of the norm is negative indicating that ^1D is closer to $^1D_{HF}$ even more so than in the state with zero field strength) and against the dipole ($\theta = \pi$) the system gets more correlated and entangled (the difference of the norm is positive indicating that ^1D is farther away to $^1D_{HF}$ even more so than in the state with zero field strength).

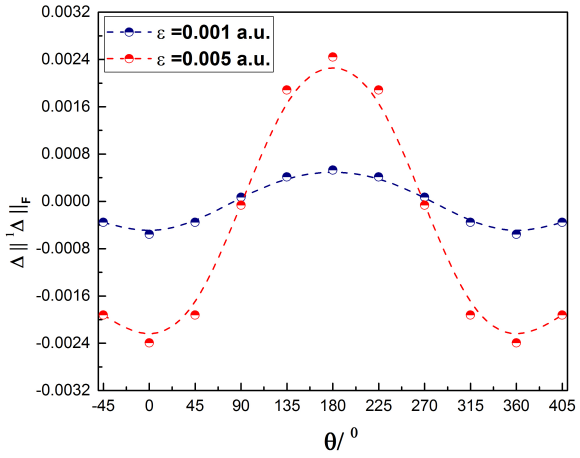

Figure 4.2: For BH the change in the angular trend for Frobenius norm ($||^1D - ^1D_{HF}||_F$) with respect to application of an electric field (ϵ). The difference in the norm is computed with respect to the state with zero-electric field hence $\Delta||^1\Delta||_F$. We see that along the direction of the dipole ($\theta = 0$), the system is decorrelated with the norm being less than even its value at zero field (hence negative). The reverse happens against the dipole ($\theta = \pi$)

To rationalize the behavior

For both HeH^+ and MgH^+ the first-order Rényi entropy as a function of the field strength

along and against the dipole moment is shown in Table I . As predicted by the theorem in section 4.2, the electron correlation, measured by the entropy, increases with the electric field in the direction against the dipole moment and decreases with the electric field in the direction of the dipole moment. While not shown, the Euclidean distance from the center of the 1-RDM set showed similar correlation trends as the entropy. The 1-RDM moves towards a non-interacting extreme point of the set as the expectation value of the one-body dipole moment increases. Figure 2 also shows that for HeH^+ the expectation value of the Coulomb repulsion between a pair of electrons $1/r_{12}$ decreases with the field strength in the direction of the dipole moment $\theta = 0$ and increases with the electric field against the direction against the dipole moment $\theta = \pi$, which is consistent with previous work showing a statistical relationship between r_{12} expectation values and electron correlation [51].

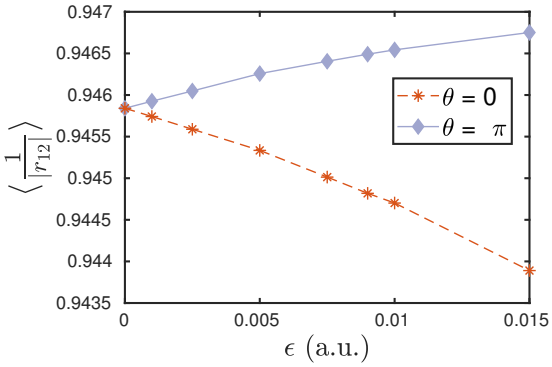

Figure 4.3: For HeH^+ the expectation value of the Coulomb repulsion between a pair of electrons $1/r_{12}$ decreases with the field strength in the direction of the dipole moment $\theta = 0$ and increases with the electric field against the direction against the dipole moment $\theta = \pi$.

Table II displays the change in the energies, dipole moments, and entropies of BH, HCN, H_2O, and HF with electric-field strength. The entropy decreases with the electric field in the direction of the dipole moment while the entropy increases with the electric field in the direction against the dipole moment. Figure 3 shows an approximately linear relationship between the change in the dipole moment and the change in the first-order Rényi entropy relative to the Rényi entropy at $\epsilon = 0$. While the computed results are approximately linear

Table 4.1: Dipole moments and entropies of HeH^+ and MgH^+ in the electric field (ϵ) are presented from p2-RDM calculations using the augmented cc-pVDZ basis set. The entropy decreases with the electric field in the direction of the dipole moment while the entropy increases with the electric field in the direction against the dipole moment. The changes in dipole moment and Rényi entropy are reported relative to zero-field values. Dipole moments are expressed in units of Debye (D), and the Rényi entropies are dimensionless.

	ϵ(a.u.)	$\lvert\mu\rvert$	S_1	$\Delta\lvert\mu\rvert$	ΔS_1
HeH^+	0.015	1.9296	0.1316	0.1614	-0.0014
	0.010	1.8705	0.1321	0.1023	-0.0009
	0.000	1.7682	0.1330	0.0000	0.0000
	-0.010	1.6795	0.1333	-0.0887	0.0003
	-0.015	1.6389	0.1338	-0.1293	0.0008
MgH^+	0.015	4.7615	0.3449	1.1779	-0.0588
	0.010	4.4078	0.3602	0.8242	-0.0435
	0.000	3.5836	0.4037	0.0000	0.0000
	-0.010	2.5031	0.4763	-1.0805	0.0726
	-0.015	1.8224	0.5281	-1.7612	0.1244

and monotonic, the theoretical results presented in the previous section do not require this relationship to be linear or even strictly monotonic.

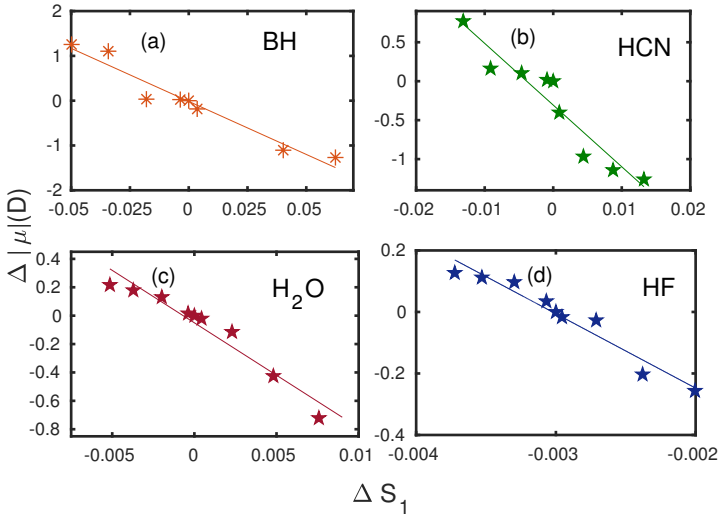

Figure 4.4: The dipole moment relative to its value at $\epsilon = 0$ versus the first-order Rényi entropy relative to its value at $\epsilon = 0$ is shown for each of the molecules (a) BH, (b) HCN, (c) H_2O, and (d) HF. The data indicates an approximately linear relationship. For BH the Pearson correlation coefficient is 0.981 and the slope of the best-fit line is -23.69 a.u.

Similar results are obtained for the molecule formaldehyde. We apply a homogeneous one-

Table 4.2: Dipole moments and entropies of molecular systems in the electric field (ϵ) are presented from p2-RDM calculations using the augmented cc-pVDZ basis set. The entropy decreases with the electric field in the direction of the dipole moment while the entropy increases with the electric field in the direction against the dipole moment. The changes in dipole moment and Rényi entropy are reported relative to zero-field values. Dipole moments are expressed in units of Debye (D), and the Rényi entropies are dimensionless.

	ϵ(a.u.)	$\|\mu\|$ (D)	S_1	$\Delta\|\mu\|$ (D)	ΔS_1
BH	-0.015	0.1036	1.0330	-1.2682	0.0626
	-0.005	1.0499	0.9903	-0.3219	0.0199
	0.000	1.3718	0.9704	0.0000	0.0000
	0.005	1.7156	0.9525	0.3438	-0.0179
	0.015	2.6268	0.9205	1.2550	-0.0499
HCN	-0.015	1.8065	1.4970	-1.2605	0.0132
	-0.005	2.1001	1.4882	-0.9669	0.0044
	0.000	3.0670	1.4838	0.0000	0.0000
	0.005	3.1707	1.4791	0.1037	-0.0046
	0.015	3.8377	1.4707	0.7707	-0.0131
H_2O	-0.015	1.3462	0.8144	-0.7215	0.0076
	-0.005	1.9534	0.8091	-0.1143	0.0023
	0.000	2.0677	0.8068	0.0000	0.0000
	0.005	2.1985	0.8048	0.1308	-0.0020
	0.015	2.2842	0.8017	0.2165	-0.0051
HF	-0.015	1.6620	0.6404	-0.2564	0.0050
	-0.005	1.8913	0.6368	-0.0271	0.0014
	0.000	1.9184	0.6354	0.0000	0.0000
	0.005	2.0155	0.6339	0.0971	-0.0015
	0.015	2.0454	0.6317	0.1270	-0.0037

dimensional electric field of strength starting from 10^5-10^8 V/m, as used in experiment [52] and proceeding to 10^9 V/m. Table III shows that both the first-order and second-order Rényi entropies decrease with the electric field in the direction of the dipole moment while they increase with the electric field in the direction against the dipole moment. Importantly, the modulation of the electron correlation by the electric field is applicable to not only individual molecules but also clusters of molecules.

Clusters of formaldehyde molecules have been employed in cold-temperature experiments, first reported in 2003 [53] and perfected in 2016 using an electrostatic Sisyphus trap [52]. We consider the two-dimensional lattice of six formaldehyde molecules separated by 5.0 Å shown schematically in Fig. 4. As for the single formaldehyde molecule, Table III reveals that the

Rényi entropies of the cluster decrease with the electric field in the direction of the dipole moment while they increase with the electric field in the opposite direction. Significantly, as displayed in Fig. 5, the increase or decrease in the entanglement of the cluster system is amplified compared to that of the individual molecules at infinite separation. The electric field controls not only the electron correlation within the molecule but also the electronic entanglement of formaldehyde molecules.

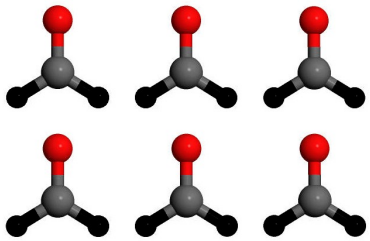

Figure 4.5: Schematic of the $(CH_2O)_6$ crystal from Jmol [54] is shown. The oxygen atoms are marked in red, the carbon atoms in grey and the hydrogens in black.

Table 4.3: Changes in the dipole moments and entropies of CH_2O and $(CH_2O)_6$ are reported as functions of the electric field ϵ relative to their values at zero field $\epsilon = 0$. In both cases the entropy decreases with the electric field in the direction of the dipole moment but increases with the electric field in the direction against the dipole moment. Dipole moments are expressed in units of Debye (D), and the Rényi entropies are dimensionless. The zero-field dipole moments of CH_2O and $(CH_2O)_6$ are 2.4263 D and 13.9403 D respectively. The 1-RDMs were computed from the a cc-pVDZ basis set using p2-RDM.

	ϵ (a.u.)	$\Delta\lvert\mu\rvert$ (D)	ΔS_1	ΔS_2
CH_2O	-0.015	-0.6337	0.0224	0.0007
	-0.005	-0.0808	0.0081	0.0002
	0.000	0.0000	0.0000	0.0000
	0.005	0.3407	-0.0064	-0.0003
	0.015	1.1097	-0.0208	-0.0007
$(CH_2O)_6$	-0.015	-3.8415	0.1517	0.0008
	-0.005	-2.6110	0.0484	0.0003
	0.000	0.0000	0.0000	0.0000
	0.005	1.5238	-0.0384	-0.0002
	0.015	4.2936	-0.1427	-0.0007

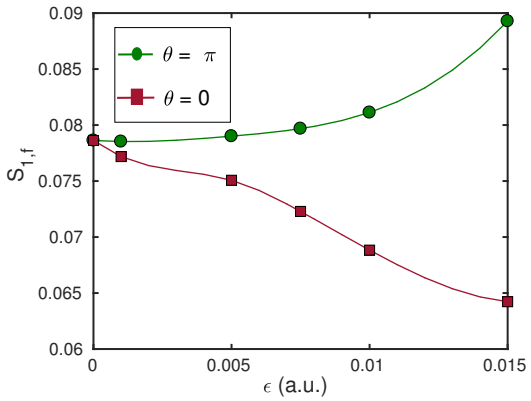

Figure 4.6: The first-order Rényi entropies S_1 of the six noninteracting molecules and the cluster are shown as functions of the electric field in the direction of the dipole moment ($\theta = 0$) and in the direction opposite to the dipole moment ($\theta = \pi$). The cluster disentangles and entangles more in the field than the six noninteracting molecules, which indicates that the field cannot only decorrelate (correlate) the individual molecules but also disentangle (entangle) the molecules from each other.

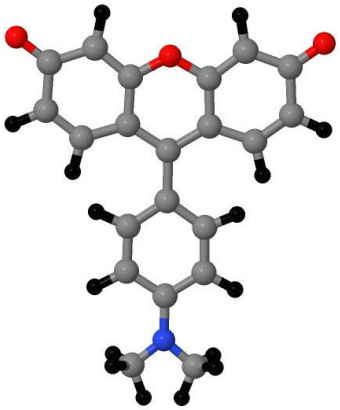

Figure 4.7: A fluorescent dye mimic of VF2.1.H is shown.

We also examined the effect of the electric field on the electron correlation of larger molecules such as a fluorescent dye mimic of VF2.1.H [55, 56], which has been used for sensing voltage in neurons [56]. Figure 6 displays the fluorescent dye mimic of VF2.1.H [55, 56]. Table IV presents the first-order Rényi entropy as a function of the field strength along and against the dipole moment . As seen in the other molecular systems, the electron correlation, measured by the entropy, increases with the electric field in the direction against the dipole moment and decreases with the electric field in the direction of the dipole moment. The

Table 4.4: Changes in the dipole moments and entropies of a fluorescent dye mimic of VF2.1.H are reported as functions of the electric field ϵ relative to their values at zero field $\epsilon = 0$. The entropy decreases with the electric field in the direction of the dipole moment but increases with the electric field in the direction against the dipole moment. Dipole moments are expressed in units of Debye (D), and the Rényi entropies are dimensionless.

ϵ(a.u.)	$\lvert\mu\rvert$	$\Delta\lvert\mu\rvert$ (D)	S_1	ΔS_1
0.0100	42.4705	13.3129	12.3920	-0.1372
0.0075	40.2996	11.1419	12.4238	-0.1054
0.0050	38.6528	4.6908	12.4600	-0.0692
0.0010	29.3534	0.7957	12.5139	-0.0153
0.0000	29.1576	0.0000	12.5292	0.0000
-0.0010	26.6115	-2.5461	12.5451	0.0158
-0.0050	23.1638	-5.9938	12.6284	0.0992
-0.0075	18.3631	-10.7947	12.6960	0.1669
-0.0100	17.0677	-12.0899	12.7674	0.2382

change in entropy reflects the movement of the 1-RDM towards a non-interacting extreme point of its N-representable set as the expectation value of the one-body dipole moment increases.

4.4 Discussion and Conclusions

The degree of electron correlation and entanglement in quantum molecular systems can be controlled through an external stimulus such as an electric field. We proved that any external stimulus that significantly changes the expectation value of a one-electron operator with non-degenerate minimum and maximum eigenvalues can be used to control the degree of electron correlation in the molecule. To obtain this result, we employed the convexity of the set of 1-RDMs and Coleman's theorem that the extreme 1-RDMs of the set are the uncorrelated 1-RDMs whose N-electron wavefunctions are Slater determinants. Using the electric field, for example, to steer the 1-RDM in the direction of the extreme 1-RDM where the dipole moment reaches its maximum value causes the quantum system to decorrelate.

The control of quantum molecular systems was demonstrated computationally with HeH^+, MgH^+, BH, HCN, H_2O, HF, CH_2O, a fluorescent dye, as well as an array of six

CH_2O. Using the first-order and second-order Rényi entropies to quantify the degree of correlation, we observed that degree of correlation could be decreased or increased through the application of a homogeneous electric field in the direction parallel or anti-parallel to the molecule's intrinsic dipole moment. Using other metrics to quantify the electron correlation, such as the distance of the 1-RDM to the center of the convex set [57], led to the same conclusions. The calculations with an array of formaldehyde molecules also showed that field can control not only the electron correlation of a formaldehyde molecule but also the entanglement among formaldehyde molecules in an array. Thereby, the external stimulus can also be employed to entangle or disentangle a set of molecules assembled by intermolecular forces in a cluster or synthetically by an optical trap. The control of a molecule's correlation and entanglement by an electric field has potential applications to designing molecules and materials with targeted properties, modifying the degree of correlation between fundamental units in quantum computation, and understanding the electric-field properties of biological systems, especially membranes.

4.5 References

[1] F. Jensen, *Computational Chemistry* (Wiley, New York, 2006).

[2] S. Kais, in *Reduced-Density-Matrix Mechanics - with Applications to Many-Electron Atoms and Molecules*, edited by D. A. Mazziotti (Wiley, New York, 2007), vol. 134 of *Advances in Chemical Physics*, pp. 493–535.

[3] D. A. Mazziotti, Phys. Rev. A **57**, 4219 (1998).

[4] C. Brif, R. Chakrabarti, and H. Rabitz, New Journal of Physics **12**, 075008 (2010).

[5] H. Rabitz, R. de Vivie-Riedle, M. Motzkus, and K. Kompa, Science **288 (5467)**, 824 (2000).

[6] D. J. Tannor and S. A. Rice, J. Chem. Phys. **83**, 5013 (1985).

[7] A. P. Peirce, M. A. Dahleh, and H. Rabitz, Phys. Rev. A **37**, 4950 (1988).

[8] A. J. Coleman, Rev. Mod. Phys. **35**, 668 (1963).

[9] R. Chakraborty and D. A. Mazziotti, Phys. Rev. A **89**, 042505 (2014).

[10] R. E. Borland and K. Dennis, J. Phys. B **5**, 7 (1972).

[11] C. Schilling, D. Gross, and M. Christandl, Phys. Rev. Lett. **110**, 040404 (2013).

[12] D. A. Mazziotti, ed., *Reduced-Density-Matrix Mechanics: With Application to Many-Electron Atoms and Molecules*, no. 134 in Advances in Chemical Physics (Wiley, New York, 2007).

[13] A. J. Coleman and V. I. Yukalov, *Reduced Density Matrices: Coulson's Challenge, Chapter 4* (Springer, New York, 2000).

[14] R. T. Rockafellar, *Convex Analysis*, Princeton Landmarks in Mathematics and Physics (Princeton University Press, 1996).

[15] D. Healion, Y. Zhang, J. D. Biggs, N. Govind, and S. Mukamel, J. Phys. Chem. Lett. **3**, 2326 (2012).

[16] D. A. Mazziotti, Chem. Phys. Lett. **289**, 419 (1998).

[17] D. A. Mazziotti, Int. J. of Quant. Chem. **70**, 557 (1998).

[18] W. Kutzelnigg and D. Mukherjee, J. Chem. Phys. **110**, 2800 (1999).

[19] W. Slebodziski, *Exterior Forms and their Applications* (Polish Scientific Publishers, Warsaw, 1970).

[20] A. E. Raeber and D. A. Mazziotti, Phys. Rev. A **92**, 052502 (2015).

[21] C. Valdemoro, Phys. Rev. A **45**, 4462 (1992).

[22] P. Ziesche, Int. J. Quantum Chem. **56**, 363 (1995).

[23] J. von Neumann, *Mathematical Foundations of Quantum Mechanics*, Princeton Landmarks in Mathematics and Physics (Princeton University Press, 1955).

[24] A. Rényi, in *Proceedings of the Fifth Berkeley Symposium on Mathematical Statistics and Probability, Volume 1: Statistics* (University of California Press, Berkeley, Calif., 1967), pp. 531–543.

[25] L. Amico, R. Fazio, A. Osterloh, and V. Vedral, Rev. Mod. Phys. **80**, 517 (2008).

[26] R. Horodecki, P. Horodecki, M. Horodecki, and K. Horodecki, Rev. Mod. Phys. **81**, 865 (2009).

[27] E. H. Wichmann, J. Math. Phys. **4**, 884 (1963).

[28] E. G. Larson, Int. J. Quantum Chem. **7**, 853 (1973).

[29] A. N. Tripathi, R. P. Sagar, R. O. Esquivel, and V. H. Smith, Jr., Phys. Rev. A **45**, 4385 (1992).

[30] G. C. Ghirardi and L. Marinatto, Phys. Rev. A **70**, 012109 (2004).

[31] Z. Huang and S. Kais, Chem. Phys. Lett. **413**, 1 (2005).

[32] T. Juhász and D. A. Mazziotti, J. Chem. Phys. **125**, 174105 (2006).

[33] A. V. Luzanov and O. Prezhdo, Mol. Phys. **105**, 2879 (2007).

[34] D. R. Alcoba, R. C. Bochicchio, L. Lain, and A. Torre, J. Chem. Phys. **133**, 1441 (2010).

[35] L. Greenman and D. A. Mazziotti, J. Chem. Phys. **134**, 034111 (2011).

[36] K. Boguslawski and P. Tecmer, Int. J. Quantum Chem. **115**, 1289 (2015).

[37] D. A. Mazziotti, Phys. Rev. Lett. **101**, 253002 (2008).

[38] D. A. Mazziotti, Phys. Rev. A **81**, 062515 (2010).

[39] D. A. Mazziotti, Chem. Rev. **112**, 244 (2012).

[40] C. A. Schwerdtfeger and D. A. Mazziotti, J. Chem. Phys. **137**, 034107 (2012).

[41] A. M. Sand, C. A. Schwerdtfeger, and D. A. Mazziotti, J. Chem. Phys. **85**, 034112 (2012).

[42] E. P. Hoy, C. A. Schwerdtfeger, and D. A. Mazziotti, J. Phys. Chem. A **117**, 1817 (2013).

[43] A. M. Sand and D. A. Mazziotti, J. Chem. Phys. **244102**, 138 (2013).

[44] A. J. Valentine and D. A. Mazziotti, J. Phys. Chem. A **117**, 9746 (2013).

[45] D. Feller, J. Comp. Chem. **17**, 1571 (1996).

[46] K. L. Schuchardt, B. T. Didier, T. Elsethagen, L. Sun, V. Gurumoorthi, J. Chase, J. Li, and T. L. Windus, J. Chem. Inf. Model. **47**, 1045 (2007).

[47] T. Dunning, Jr., J. Chem. Phys. **53**, 2823 (1970).

[48] P. Jizba and T. Arimitsu, Phys. Rev. E **69**, 026128 (2004).

[49] F. Franchini, A. R. Its, and V. E. Korepin, J. Phys. A **41**, 025302 (2008).

[50] R. Islam, R. Ma, P. M. Preiss, M. E. Tai, A. Lukin, M. Rispoli, and M. Greiner, Nature **528**, 77 (2015).

[51] M. Nest, M. Ludwig, I. Ulusoy, T. Klamroth, and P. Saalfrank, J. Chem. Phys. **138**, 164108 (2013).

[52] A. Prehn, M. Ibrugger, R. Glockner, G. Rempe, and M. Zeppenfeld, Phys. Rev. Lett. **116**, 063005 (2016).

[53] S. A. Rangwala, T. Junglen, T. Rieger, P. W. H. Pinkse, and G. Rempe, Phys. Rev. A **67**, 043406 (2003).

[54] *Jmol: An Open-source Java Viewer for Chemical Structures in 3D* (2017), URL `http://www.jmol.org/`.

[55] E. W. Miller, J. Y. Lin, E. P. Frady, P. A. Steinbach, W. B. Kristan, and R. Y. Tsien, Proc. Natl. Acad. Sci. U.S.A. **109**, 2114 (2012).

[56] C. R. Woodford, E. P. Frady, R. S. Smith, B. Morey, G. Canzi, S. F. Palida, R. C. Araneda, W. B. Kristan, C. P. Kubiak, E. W. Miller, et al., J. Am. Chem. Soc. **137**, 1817 (2015).

[57] C. A. Schwerdtfeger and D. A. Mazziotti, J. Chem. Phys. **130**, 224102 (2009).